Journal of Hydrology 573 (2019) 60–81

Contents lists available at ScienceDirect

Journal of Hydrology

journal homepage: www.elsevier.com/locate/jhydrol

Research papers

Projecting climate change impacts on hydrological processes on the Tibetan Plateau with model calibration against the glacier inventory data and observed streamflow

Qiudong Zhao[a,b], Yongjian Ding[b,c,*], Jian Wang[d], Hongkai Gao[e], Shiqiang Zhang[f,g,*], Chuancheng Zhao[h], Junli Xu[d], Haidong Han[a,b], Donghui Shangguan[b]

[a] Key Laboratory of Ecohydrology of Inland River Basin, Cold and Arid Regions Environmental and Engineering Research Institute, Chinese Academy of Sciences, Lanzhou 73000, China
[b] State Key Laboratory of Cryospheric Sciences, Cold and Arid Regions Environmental and Engineering Research Institute, Chinese Academy of Sciences, Lanzhou 730000, China
[c] University of Chinese Academy of Sciences, Beijing 100049, China
[d] College of Urban and Plans, Yancheng Teachers University, Yancheng 224002, China
[e] School of Geographic Sciences, East China Normal University, Shanghai 200241, China
[f] Shaanxi Key Laboratory of Earth Surface System and Environmental Carrying Capacity, Northwest University, Xi'an 710127, China
[g] College of Urban and Environmental Science, Northwest University, Xi'an 710127, China
[h] College of Geography and Environmental Engineering, Lanzhou City University, Lanzhou 730070, China

ARTICLE INFO

This manuscript was handled by Marco Borga, Editor-in-Chief, with the assistance of Baptiste François, Associate Editor

Keywords:
Climate change
VIC-CAS model
Glaciers
Streamflow
Tibetan Plateau

ABSTRACT

Analyzing the impacts of climate change on hydrology and future projections of water supplies is fundamental for the efficient management and planning of water resources in large river systems on the Tibetan Plateau (TP), which is known as the "water tower of Asia." However, large uncertainties remain in the projections of streamflow and glaciers in these cryospheric catchments due to great uncertainties in climate change projection and modeling processes. In this work, we developed an extended Variable Infiltration Capacity (VIC) macroscale hydrological model (named VIC-CAS), which was coupled with glacier melting and glacier evolution schemes. A two-stage calibration procedure that used glacier inventory data and the observed streamflow was adopted to derive the model parameters. The calibrated VIC-CAS model was then used to assess the future change in glaciers and runoff using downscaled climate model data in the upstream regimes of the Yellow, Yangtze, Mekong, Salween, and Brahmaputra rivers on the TP. The results indicated that both temperature and precipitation were projected to increase, resulting in a greater than 50% decline of the glacier area by the end of the 21st century in the five catchments. Glacier runoff was already beyond its tipping point at the beginning of the 21st century with a greater than 20% loss of the glacier area except in the upstream of the Yangtze River, where glacier runoff was projected to decrease after the 2030 s. Annual streamflow was projected to increase significantly as a result of increased rainfall-induced runoff, compensating for the reduced glacier/snow melt water in the five major upstream river basins. The increasing rate of warm season streamflow was clearly less than that of annual runoff. A negative trend in warm season streamflow was expected if precipitation did not sufficiently increase. The annual hydrograph remained largely unchanged, except in the upstream of the Yellow River, where peak streamflow was predicted to occur 1 month earlier because of the earlier snowmelt and greater rainfall/precipitation ratio from May to June.

1. Introduction

The Tibetan Plateau (TP) is commonly known as Earth's third pole because it possesses both the largest and highest plateaus and covers an area of 2.5×10^6 km^2 with a mean elevation of 4500 m a.s.l. (above sea level). Due to the uniquely complex terrain and high altitude, the TP is the largest permafrost region (1.5×10^6 km^2) that exists at a mid-low latitude (Ye et al., 2013) and contains the largest number of glaciers (approximately 4, 9873 km^2) outside of the polar regions (Liu et al., 2015a). The TP, also called the "Asian water tower" contains the

* Corresponding authors at: State Key Laboratory of Cryospheric Sciences, Cold and Arid Regions Environmental and Engineering Research Institute, Chinese Academy of Sciences, Lanzhou 730000, China (Y. Ding). College of Urban and Environmental Science, Northwest University, Xi'an 710127, China (S. Zhang).
E-mail addresses: dyj@lzb.ac.cn (Y. Ding), zhangsq@lzb.ac.cn (S. Zhang).

https://doi.org/10.1016/j.jhydrol.2019.03.043
Received 1 December 2018; Received in revised form 5 March 2019; Accepted 6 March 2019
Available online 15 March 2019
0022-1694/

headwaters of several major Asian rivers, which support nearly two billion people (nearly 25% of the world's population) (Huang et al., 2012).

Over the last several decades, the surface air temperature over the TP has increased at a faster rate than that on average in the Northern Hemisphere (Wang et al., 2008; Zhong et al., 2011; Guo and Wang, 2012; Yang et al., 2014; Duan and Xiao, 2015). The cryosphere (snow, glaciers, and permafrost) on the TP is the most sensitive indicator of climate change (Lemke et al., 2007; Kang et al., 2010). Rising air temperatures are causing rapid changes in the cryosphere, including glacier shrinkage (decreased by 10%), increasing negative glacier mass balance, permafrost degradation, and thickening of the active layer of permafrost (Zhang, 2007; Li et al., 2008; Wei et al., 2014). The cryospheric change has also had considerable impacts on hydrological processes. Permafrost degradation increases infiltration, enlarges subsurface water, and leads to lower summer runoff and higher winter runoff (Ye et al., 2009; Niu et al., 2011). With accelerated glacier melting, river runoff will initially increase as a result of more meltwater, but eventually decrease due to the loss of glacier area on the TP (Yao et al., 2004; Ye et al., 2007, 2008; Gao et al., 2012; Immerzeel et al., 2010, 2012; Shi et al., 2016).

According to the Intergovernmental Panel on Climate Change Fifth Assessment Report (IPCCAR5), the air temperature over the TP is expected to increase by 1.9 °C and 4.3 °C by the end of the 21st century under RCP2.6 and RCP8.5 emission scenarios, respectively (Su et al., 2013). Glaciers in the TP are likely to recede, and the volume of glacier meltwater may dwindle in some watersheds (Immerzeel et al., 2010; Lutz et al., 2014). The near-surface permafrost area is projected to decrease by 46–81% on the TP by the end of the 21st century (Nan et al., 2005; Lawrence and Slater, 2005; Guo and Wang, 2012). Therefore, it is essential to quantify the potential effects of future climate changes on the discharges of major large rivers originating from the TP, which will benefit from water resource management for sustainable development on the TP and in downstream regions.

Numerous studies have been conducted to quantitatively investigate the impacts of climate change on hydrological processes on the TP in recent years (Rees and Collins, 2006; Fujita et al., 2007; Li et al., 2010, 2013, 2014; Tahir et al., 2011; Gao et al., 2012, 2015; Immerzeel et al., 2010, 2012; Jeelani et al., 2012; Zhang et al., 2015). Among these studies, several have focused on projecting future hydrological processes on the TP at the scale of large catchments or river-basins using hydrological models determined by the output of Global Climate Models (GCMs), some of which are listed in Table 1. Additionally, only a small number of studies have accounted for glacier melt and the response (retreat and advance) processes to climate change (Immerzeel et al., 2010; Lutz et al., 2014; Su et al., 2016), and in others, the glaciers were completely ignored (Lu et al., 2018; Liu et al., 2011, 2015b; Li et al., 2013, 2014). Although these three studies provide important insights into the future changes in the streamflow and glaciers on the TP, there has been a strong debate regarding the future trend of the streamflow, due to inconsistently simulated contributions and trends of glacier meltwater. Immerzeel et al. (2010) stated that the streamflow will likely decrease by the mid-century due to reductions in glacier meltwater in the upper Yangtze, Brahmaputra, Ganges, and Indus basins; however, they also highlighted a notable increase in runoff of the upper Yellow basin, which depends only marginally on glacier melt and increasing precipitation. Lutz et al. (2014) projected an increase in runoff until at least 2050 due to the increasing precipitation at the expense of glacier runoff in the upper Mekong, Salween, Brahmaputra, and Ganges basins and accelerated glacier melt in the upper Indus basin. Su et al. (2016) indicated that the discharge of six major upstream river basins (Yellow, Yangtze, Salween, Mekong, Brahmaputra and Indus) would remain moderately elevated in the near-term (2011–2040) and increase by 2.7–22.4% in the long-term (2041–2070) as a result of increasing precipitation and glacier meltwater, and the accelerated glacier melt is considered to be the main cause for the increased runoff in the Brahmaputra and Indus basins. Large variability and uncertainty is clearly evident in the projections of runoff and glaciers obtained via different models and model parameters for the same study catchment on the TP.

A suitable hydrological model and an effective model parameter estimation approach are prerequisites for the successful projections of hydrological processes (Chen et al., 2017a; Moradkhani et al., 2005). Hydrological models are a fundamental tool for quantitatively investigating and projecting hydrological processes, and the model schemes for snow/ice melt, glacier response, and soil freezing and thawing should be involved in simulating the hydrological conditions over the TP. Three hydrological models with glacier melt (degree-day method) and glacier response (volume-area scaling law) schemes, namely, the Snowmelt Runoff Model (SRM), the Spatial Processes in Hydrology model (SPHY) and the VIC-glacier model, were applied to simulate and project hydrological processes at the large catchment scale on the TP (Immerzeel et al., 2010; Lutz et al., 2014; Su et al., 2016). The specified relationship between glacier volume and glacier area was used to solve the changes in glacier area based on the simulated mean mass balance for glaciers in each size class (Lutz et al., 2014) or in the basin (Immerzeel et al., 2010; Su et al., 2016). The different sensitivities to climate change among glaciers of different sizes have been ignored in simulations of the glacier area change at the basin scale. Larger glaciers have a smaller surface area-to-volume ratio, so they are less sensitive to climate change than smaller glaciers (Van de Wal and Wild, 2001; Immerzeel et al., 2012). Another key issue is the oversight of the hydrological effects of frozen soil in the SRM and SPHY models, although the exclusion of the frozen soil hydrological processes could induce large errors in catchments on the TP due to the wide extent of frozen soil (Cuo et al., 2015).

Hydrological models usually contain a large number of parameters that cannot be measured directly but instead are inferred by model calibration, which adjusts the parameter values to fit the simulated runoff compared to the observations. However, a good model performance in streamflow simulations does not guarantee the reliable reproduction of other hydrological variables. For example, the underestimation of mountainous precipitation can be compensated by the overestimation of glacier meltwater, and vice versa, which has been called the "effect of error compensation" (Stahl et al., 2008; Schaefli and Huss, 2011; Duethmann et al., 2014). Therefore, more observed hydrological variables must be accounted for multi-objective calibration, especially for glacier/snow-fed catchments (Stahl et al., 2008; Shrestha et al., 2014; Chen et al., 2017a,b). For hydrological simulations in glacierized catchments, some recent studies have jointly used the observed glacier mass balances and in-situ runoff for model calibration to provide more realistic results (Stahl et al., 2008; Huss et al., 2008; Konz and Seibert, 2010; Duethmann et al., 2015; Immerzeel et al., 2012). On the data-scarce TP, the degree-day method has been widely adopted to simulate glacier melting. The snow/ice degree-day factors (*DDFs*) are the most essential parameters, and variations in these factors lead to significant changes in simulated glacier meltwater contributions to streamflow and trends in glacier runoff in the future (Zhao et al., 2015; Huss et al., 2014). However, glacier observations have not been considered for the model parameter calibration and validation in previous studies on hydrological projections at the large basin-scale on the TP (Immerzeel et al., 2010; Lutz et al., 2014). In such a region with large uncertainties in precipitation data, this oversight can lead to unrealistic or incorrect conclusions concerning glacier meltwater.

In this study, a VIC-CAS model coupled with glacier melting and glacier response schemes was developed within the framework of the VIC macroscale hydrologic model, which is a well-established, distributed land surface, hydrological model with frozen soil and snow schemes. A two-stage calibration strategy was adopted to calibrate the model parameters. First, the parameters of glacier melting were calibrated using the Chinese Glacier Inventory (CGI) data, and second, the hydrological processes were optimized using the observed streamflow

Table 1
Summary of papers related to runoff projections on the TP at the scale of large catchments or river-basins.

References	Catchment	Hydrological Model/Limitations	Major conclusions
Immerzeel et al. (2010)	Five upstream river basins (Yellow, Yangtze, Indus, Brahmaputra, and Ganges rivers) in the TP	SRM-glacier/Lack of frozen soil module; Ignore the differences in sensitivity to climate change for glaciers of different size	Although the precipitation increases, all the basins except the Yellow would have a 5.2–19.6% decrease in mean annual water supply in 2046–2065 relative to 2000–2007 because of less glacier runoff
Liu et al. (2011)	Upper Yellow river basin	SWAT/Lack of glacier module	Annual average streamflow will increase by 17.9% (11.5%), 17.9% (15.9%) and 42.9% (34.55%) in the 2020 s, 2050 s and the 2080 s under scenario A2 (B2) relative to 1961–1990 with an increase in precipitation
Li et al. (2013, 2014)	Eight branches of Brahmaputra river	Lumped SIMHYD and GR4J/ Lack of glacier and frozen soil module	The mean annual future runoff in most of catchments shows a decrease in 2046–2065 relative to 1962–2002 because of decreasing precipitation
Lutz et al. (2014)	Five upstream river basins (Mekong, Salween, Brahmaputra, Indus, and Ganges rivers) in the TP	SPHY/Lack of frozen soil module	For all basins except Indus, the glacier melt water is projected to have a slight decrease in 2041–2050 with respect to 1998–2007. The streamflow would increase by 4.5–7.5% (2.1–13.85%) under RCP4.5 (RCP8.5) emission scenarios
Liu et al. (2015b)	A tributary of Brahmaputra river (Lhasa River basin)	VIC/Lack of glacier module	The annual streamflow of Lhasa River basin increase by 6.04–13.92% in 2046–2065 relative to 1981–2000 because of increasing precipitation
Su et al. (2016)	Six upstream river basins (Yellow, Yangtze, Mekong, Salween, Indus, and Brahmaputra rivers) in the TP	VIC-glacier/Ignore the differences in sensitivity to climate change for glaciers of different size	Due to increased rainfall runoff and glacier melt water, the streamflow of the six basins would remain moderately increase in 2011–2040, and increase by 2.7–22.4% in the 2041–2070 relative to 1971–2000. In the upper Brahmaputra and Indus, more than 50.0% of the total runoff increase is from the increased glacier melt water in the long run
Lu et al. (2018)	source regions of Yellow River andYangtze RiverSource regions of Yellow and Yangtze rivers	VIC/ Lack of glacier module	Due to the precipitation increase, the streamflow of two catchments would display general increases by 3–5% in 2041–2060 relative to 1981–2000

in the five major upstream river basins (Yellow, Yangtze, Mekong, Salween, and Brahmaputra) on the TP. The calibrated VIC-CAS model was then forced with the downscaled GCM outputs to project future changes in runoff components and glaciers under RCP2.6 and RCP4.5 global emission scenarios in the five study catchments.

2. Description of the study area

The upstream regions of the Yellow River (UYE), Yangtze River (UYA), Mekong River (UM), Salween River (US), and Brahmaputra River (UB) on the TP were selected as the study area (Fig. 1). The selected basin characteristics are listed in Table 2. The five catchments cover an area of 5.97×10^4 km^2, which is approximately a quarter of the area of the TP above 2000 m a.s.l. The study basins are dominated by the Asian monsoon system during the summer (Tong et al., 2014). Nearly two-thirds of the annual precipitation occurs during the warm season, from April to September with increasing precipitation observed from northwest to southeast (Wang et al., 2018). The topography of the basins is highly variable with the elevation gradually increasing from the southeast to northwest. Moreover, the vegetation also exhibits clear horizontal variation characteristics, with forests located in the southeastern areas and grasslands/steppes presenting in both the northern and western areas (Song et al., 2004; Cui and Graf, 2009), which is caused by the topographical and climatic characteristics.

According to the first Chinese glacier inventory (FCGI), the glacier coverage of the five study catchments is less than 3%. The UB has the largest glacier area (approximately 4261 km^2, 2.1% of the UB basin), and the UYE has the lowest glacier coverage (approximately 129 km^2, only 0.1% of the basin area). Previous studies (Zhang et al., 2013; Su et al., 2016) have suggested that the contribution of glacier meltwater to stream runoff is small in the selected hydrological stations of the five catchments due to limited glacierization (Table 2). However, the role of glacier meltwater is very important to the upstream tributaries of the study catchments, where glacier meltwater accounts for 32% of the river runoff in the Tuotuo River basin, a tributary of the Yangtze River (Zhang et al., 2008). It should also be noted that permafrost occurs across an area of 29.60×10^4 km^2 and accounts for approximately half of the surface area of our study catchments. Even in the lowest

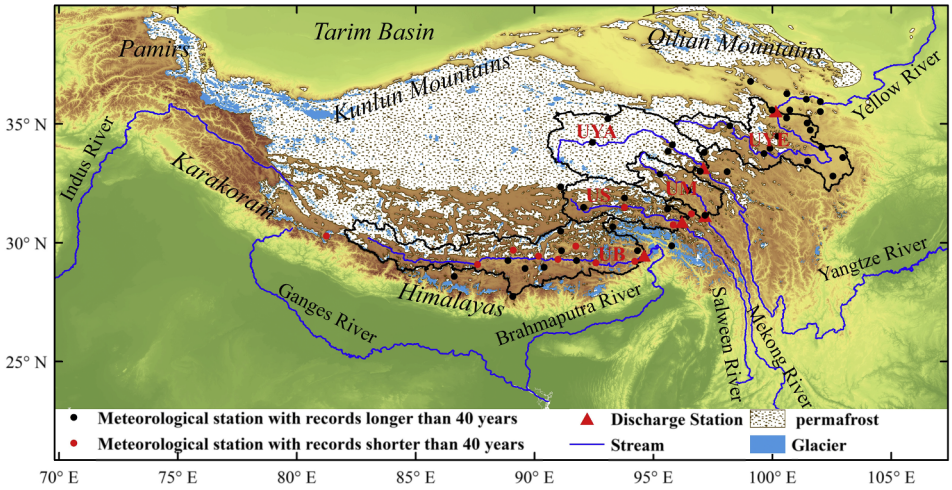

Fig. 1. Topography of the Tibetan Plateau (background), distribution of glaciers and permafrost, locations of meteorological and hydrological stations, basin boundaries, and river courses of the upstream regions of the Yellow, Yangtze, Mekong, Salween and Brahmaputra rivers (the glacier and permafrost data are from http://westdc.westgis.ac.cn. The locations of the stations are from http://data.cma.cn).

Table 2
Characteristics of the five upstream river basins on the TP.

	Yellow	Yangtze	Mekong	Salween	Brahmaputra
Station	Tangnaihai	Zhimenda	Changdu	Jiayuqiao	Nuxia
Catchment area (km^2)	123,023	140,073	53,644	75,506	204,863
Glacier area (km^2)	129	1249	219	1041	4261
Permafrost area (km^2)	42,121	134,731	20,521	31,563	67,112
Period of observed discharge	1971–2010	1971–2009	1971–2000	1980–1985	1971–1999

permafrost watershed, UB, the permafrost area reaches up to 6.7×10^4 km^2, accounting for 32.7% of the basin area. Thus, the frozen soil hydrological processes should not be neglected in the hydrological simulation of the catchments.

3. Data and methodology

3.1. VIC-CAS model description

The degree-day method and glacier volume-area scaling law were coupled to the VIC model (version 4.2.d) to simulate glacier melt and glacier area change based on our previous studies (Zhao et al., 2013, 2015; Zhang et al., 2012; Gao et al., 2017a,b). The glacier mass balance was calculated on a daily time-step, while the glacier area was updated on an annual time-step.

3.1.1. Brief description of the VIC model

The VIC model is a physically based, large-scale, distributed land surface hydrological model (Liang et al., 1996), and it is used to calculate full energy and water budgets within each grid cell at daily or sub-daily time steps considering the snow accumulation, snow melt, and soil freeze and thaw processes (Liang et al., 1996; Nijssen et al., 2001; Cherkauer and Lettenmaier, 2003; Elsner et al., 2010; Gao et al., 2009). The model has been widely applied in regional and global hydrological studies at a spatial resolution between 1/8° and 2° (Nijssen et al., 2001; Dan et al., 2012; Hidalgo et al., 2013; Zhang et al., 2013; Elsner et al., 2014; Su et al., 2016; Zhao et al., 2013, 2015). The VIC model can be forced by either daily or sub-daily meteorological data. Daily precipitation, daily maximum and minimum air temperatures, and daily average windspeed data are required to run the model so that the VIC model can be used for discharge simulations in the data-scarce mountain watersheds.

3.1.2. Glacier schemes

3.1.2.1. Setting model calculated unit. The VIC model usually adopts the rectangular grid as a calculated cell and runs within each cell independently. The model settings may place a glacier in two different cells, making it difficult to obtain each glacier mass balance and thus calculate the glacier area change because the volume-area scaling relation is only suitable for individual or several glaciers and not for a part of a glacier. Considering the ridge lines are usually boundaries of glaciers and sub-basins, we adopted the sub-basin as a model calculated unit to localize each glacier in a separate calculated unit (Fig. 2).

3.1.2.2. Fraction of glacier coverage. To account for mountain glacier melt and its influence on hydrology, a new land cover type designated "glacier" was introduced into the calculated unit mosaic of the VIC model in addition to ice-free land. Glaciers usually form in higher elevation zones with lower air temperatures and higher relative humidity. For accurate estimation of glacier melting, glaciers were subdivided into intervals of 100 m by sets of elevation bands (called glacier bands) within a model calculated unit. The mean elevation of each glacier band was generated from high-resolution Digital Elevation Model (DEM) data. The fraction of the calculated unit covered by each glacier at each glacier band was calculated based on glacier outlines and DEM data (Fig. 3). To consider the impact of the surface aspect on glacier melt, the mean cosine of the surface aspect for each glacier within each elevation band was calculated (Fig. 3).

3.1.2.3. Atmospheric sub-grid variability for glaciers. In this study, the mean elevation of each glacier band was used to lapse the ice-free zone mean temperature and precipitation in the calculated unit to obtain more accurate local estimates according to the following algorithm:

$$T_{band} = T_0 + T_{alt,m} \times (E_{band} - E_0) \quad (1)$$

$$P_{band} = P_0 \left[1 + \frac{P_{alt,m} \times (E_{band} - E_0)}{P_{0,m}} \right] \quad (2)$$

where T_{band} and P_{band} are the daily mean air temperature (°C) and precipitation (mm) in the glacier elevation band, respectively; T_0 and P_0 are the daily mean air temperature (°C) and precipitation (mm) of ice-free land in the calculated unit, respectively; E_{band} and E_0 are the mean elevations (m) of the glacier band and the ice-free land in the calculated unit, respectively; $T_{alt,m}$ and $P_{alt,m}$ are the respective corresponding monthly temperature lapse rate (°C m^{-1}) and precipitation gradient (mm m^{-1}); $P_{0,m}$ is the mean corresponding monthly precipitation (mm) of ice-free land in the calculated unit within the historical time period when we calculated the precipitation gradient; and the subscript m represents the month. If the calculated P_{band} is less than zero, then the value of P_{band} is set to zero.

3.1.2.4. Glacier melting and area evolution model. During the past several decades, energy-balance and temperature-index methods have been developed and widely used to simulate glacier melt around the world (Hock, 2005; Hock and Holmgren, 2005; Zhang et al., 2012). Although the energy-balance models have a solid physical basis, they are often difficult to apply in data-scarce mountain catchments where the data required for the model are not always available. The simple temperature-index or degree-day approaches are widely used to estimate snow/ice melt with sufficient accuracy for most purposes due to the readily availability of air temperature data and computational simplicity (Huss et al., 2008; Carenzo et al., 2009; MacDougall et al., 2011; Gao et al., 2012; Zhao et al., 2015). In this study, we adopted the extended degree-day algorithms to calculate glacier melt in each glacier band considering the exposure dependence of the degree-day factor on the surface aspect (Konz et al., 2007; Immerzeel et al., 2012; Zhao et al., 2015):

$$M_{i,band} = \begin{cases} DDF_{snow/ice} \times (1 - R_{exp} \times cosasp_{i,band}) \times T_{band} & T_{band} > 0.0 \\ 0 & T_{band} \le 0.0 \end{cases} \quad (3)$$

where $M_{i,band}$ is the total melt of snow/ice (mm) for glacier i in the $band^{th}$ glacier band; $DDF_{snow/ice}$ is the degree-day factor for snow/ice (mm °C^{-1} day^{-1}); R_{exp} is the factor quantifying the aspect dependence of $DDF_{snow/ice}$; and $cosasp_{i,band}$ is the mean cosine of the surface aspect for glacier i within the elevation band.

The key element of the glacier scheme is the simulation of glacier retreat or advance. There are two main approaches for simulating the glacier area evolution. The most physically rigorous method is the numerical ice-flow models. However, this approach requires detailed

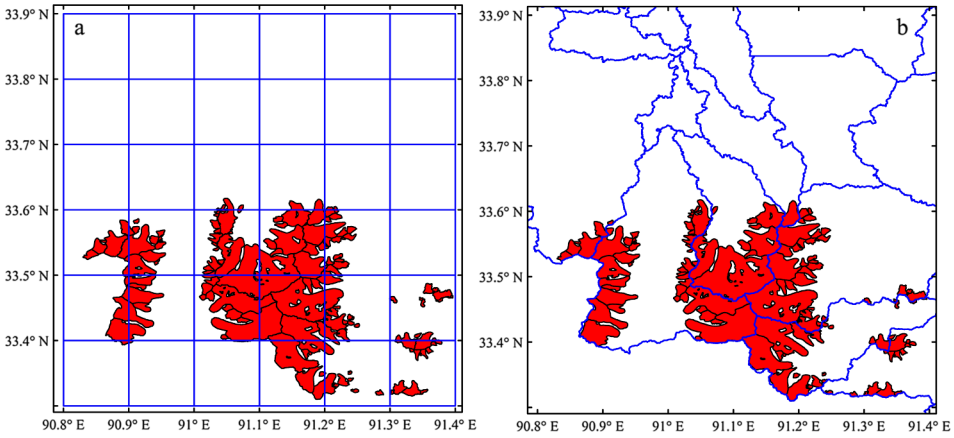

Fig. 2. Spatial distribution of glaciers in 0.1° × 0.1° rectangular grids (a) and sub-basins (b).

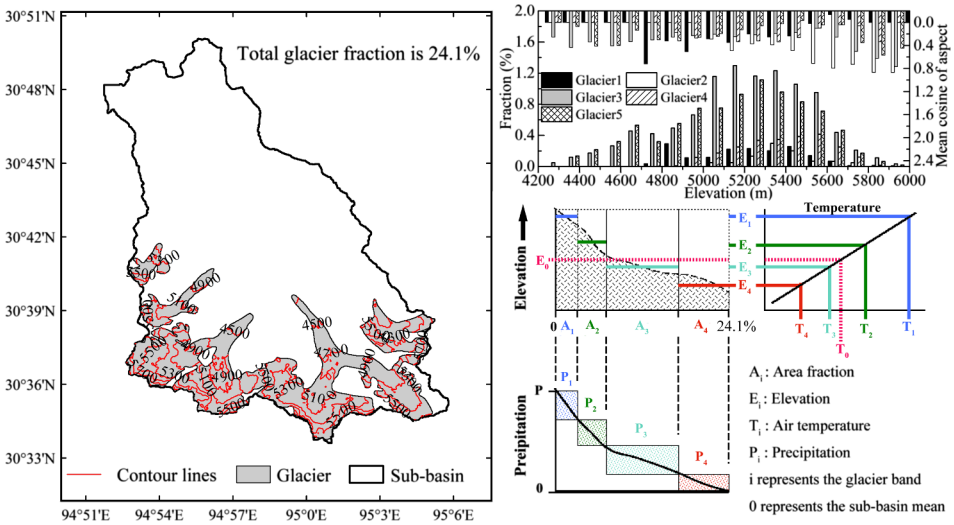

Fig. 3. Representation of glaciers in the sub-basin calculated unit of VIC-CAS.

information on the glacier surface and bed geometry, therefore, is not well-suited for extensive data-scarce regions. Hence, the simple volume-area scaling approach has been widely applied to simulate changes in glacier area based on the simulated mass balance (Radić et al., 2007; Stahl et al., 2008; Raper and Braithwaite, 2006; Immerzeel et al., 2010; Lutz et al., 2014; Su et al., 2016). In this study, the glacier area evolution was simulated by combining the simulated mass balance with the volume-area scaling law, which was derived from the measured size of alpine glaciers around the globe (Liu et al., 2003; Raper and Braithwaite, 2005; Kotlarski et al., 2010; Grinsted, 2013):

$$V = cA^{\gamma} \tag{4}$$

$$A = (V/c)^{\frac{1}{\gamma}} \tag{5}$$

where V and A are the glacier volume (km^3) and area (km^2) of each glacier in the model calculated unit, respectively, and the constant $c = 0.0365$ and dimensionless scaling coefficient $\gamma = 1.375$ were obtained from Radić and Hock (2010).

The initial glacier volume and average glacier thickness were estimated from the initial glacier area using Eqs. (4) and (5). The volume of each glacier was updated by adding the calculated change in volume, which was determined from the annual mass balance, on September 30 (the end date of the hydrological year) every year. The new glacier area (A_{new}) was computed using the volume-area scaling law (Eq. (5)). The area change of each glacier (ΔA) was computed as follows:

$$\Delta A = A_{new} - A_{old} \tag{6}$$

Then, the area fraction of each glacier in the elevation bands was adjusted followed by the change in glacier area. We assume that the glacier advances or retreats in the lowest glacier elevation band first, which has been shown to be reasonable by analyses of the spatial changes in glaciers from 1999 and 2004 in the Western Himalaya (Berthier et al., 2007). When the glacier retreats, the glacier area of the lowest band shrinks. If the calculated shrinking area of the glacier is greater than that of the glacier in the lowest elevation band, then the glacier area of the lowest band will be set to zero and the glacier area in the neighboring upper elevation band will be decreased to the remaining area. In contrast, when the glacier advances, the glacier area of the lowest glacierized band will be increased. However, the increasing glacier area in the lowest glacierized elevation band is limited by the maximum capacity, which is set to the initial input glacier area, except for the initial lowest elevation band. If the calculated increasing glacier area is sufficiently great, the neighboring lower elevation band will need to be included. We adopted a glacier-adjusted method similar to that used by Möller and Schneider (2010) and Zhang et al. (2012).

3.1.3. Routing scheme

The separate Lohmann routing module (Lohmann et al., 1996, 1998) was used as a postprocessor in the VIC model package for the routing of streamflow from the land surface simulation of grid cells. In this study, the land surface simulation was modified on a sub-basin scale. To use the Lohmann routing model to calculate streamflow, some modifications in code and input data were necessary. First, sub-basins were identified

using the Pfafstetter coding system, which determines the routing order of the sub-basins and contains topographic information of the river network. Within a given sub-basin, geographic information system software was used to calculate the area and downstream distance to the outlet of the sub-basin along the flow direction. Finally, the modified Lohmann routing model was used to calculate the water recharge from each sub-basin to the outlet of the river basin from the land surface simulation, area, routing order and routing distance of the sub-basins.

3.2. Data description

3.2.1. Glacier data

The FCGI and second Chinese Glacier Inventory (SCGI) have been completed and released by the Cold and Arid Region Environmental and Engineering Research Institute of the Chinese Academy of Sciences (CAREERI). The FCGI was completed based on topographical maps and aerial photographs acquired from the 1960s to 1980s (Shi et al., 2009), among which the most photographs were acquired in the 1970s. The SCGI was compiled based on remote-sensing images after 2004, including Landsat TM/ETM+ and ASTER images, and SRTM digital elevation models (Liu et al., 2015a; Guo et al., 2015). The SCGI covers 86% of the glacierized area of China. The remaining regions are mainly located on the southeastern TP, which covers part of the southern region of the upstream part of the Salween River and Brahmaputra River.

The spatial distribution of glaciers from the FCGI was used to calculate the initial glacier input data. The updated glacier distribution datasets of SCGI were used to calibrate and validate the glacier model parameters, including degree-day factors ($DDF_{snow/ice}$) and the factor quantifying the aspect dependence (R_{exp}) of the $DDF_{snow/ice}$.

3.2.2. Interpolation of meteorological forcing data

Daily atmospheric data (maximum, minimum, and mean temperatures, precipitation, as well as wind speed) are required to force the VIC-CAS model. The observed meteorological dataset of 54 national meteorological stations inside or around our study catchments (Fig. 1) was used for the daily spatial interpolation. These weather stations lie between latitudes 27°44′N and 36°47′N and longitudes 81°15′E and 102°58′E, with a wide elevation range spanning from 2085 m to 4800 m. The data were collected from the National Climate Center of the China Meteorological Administration and consisted of daily values from January 1961 to December 2010. The dataset was created from in-situ observations applying firm quality control, including internal temporal and spatial consistency checks, homogeneity tests, and potential outlier detection (Feng et al., 2004; Ding et al., 2008). The dataset was also regarded as the most credible meteorological dataset in China. All selected stations have records longer than 30 years, and 43 stations have acquired continuous daily data over the 40-year period from 1971 to 2010.

Temperature and precipitation have considerable spatial variations due to the effects of geographical factors, different water vapor sources and the climate dominated area in these large-scale catchments on TP (Su et al., 2016). In this study, the 'Gradient plus Inverse-Distance-Squared' (GIDS) algorithm was employed to interpolate the air temperature and precipitation data considering the different effects of geographical factors (latitude, longitude and elevation) (Price et al., 2000):

$$T_0 = \left[\sum_{i=1}^{n} \frac{1}{d_i^2}\right]^{-1} \sum_{i=1}^{n} \left\{\frac{1}{d_i^2}[T_i + T_{alt,m}(E_0 - E_i) + T_{lat,m}(lat_0 - lat_i) + T_{lon,m}(lon_0 - lon_i)]\right\} \quad (7)$$

$$P_0 = \left[\sum_{i=1}^{n} \frac{1}{d_i^2}\right]^{-1} \sum_{i=1}^{n} \left\{\frac{P_i}{d_i^2}[1 + (P_{alt,m}(E_0 - E_i) + P_{lat,m}(lat_0 - \mathrm{lat}_i) + P_{lon,m}(lon_0 - lon_i))/P_{i,m}]\right\} \quad (8)$$

where T_0 and P_0 are the daily air temperature (°C) and precipitation (mm) of ice-free land in the predicted model calculated unit, respectively; T_i and P_i are the observed daily air temperature and precipitation at the *ith* neighboring weather station, respectively; E_0, lat_0, and lon_0 are the mean elevation (m), latitude (°), and longitude (°) of ice-free land in the calculated cell, respectively; E_i, lat_i, and lon_i are the elevation (m), latitude (°), and longitude (°) of *ith* neighboring weather station, respectively; d_i is the distance between weather station i and the predicted grid point; $P_{i,m}$ is the mean monthly precipitation at neighboring weather station i (mm) within the historical time period when the precipitation gradients were calculated; n is the number of neighboring stations, which was set to 3 in this study; and $T_{alt,m}$ (°C/m), $T_{lat,m}$ (°C/°), $T_{lon,m}$ (°C/°), $P_{alt,m}$ (mm/m), $P_{lat,m}$ (mm/°), and $P_{lon,m}$ (mm/°) are the air temperature and precipitation gradients in response to elevation, latitude, and longitude, respectively.

The daily wind speed of each calculated cell was interpolated from observations of the three nearest stations using the IDW (Inverse-Distance-Squared) method:

$$W_0 = \left[\sum_{i=1}^{n} \frac{1}{d_i^2}\right]^{-1} \sum_{i=1}^{n} \left(\frac{1}{d_i^2} \times W_i\right) \quad (9)$$

where W_0 is the daily wind speed at the model calculated unit (m/s), and W_i is the daily observed wind speed at a neighboring weather station i (m/s).

Considering the remarkable differences in water vapor transport among the five catchments (Cuo et al., 2013; Gao et al., 2014; Guo et al., 2016), the air temperature and precipitation gradients were computed individually for each catchment. A multiple linear regression analysis was used to calculate the gradients from the observations and geographical factors of meteorological stations inside and adjacent to the catchment. Table 3 summarizes the monthly precipitation gradients in response to elevation, longitude and latitude. The spatial distribution of our calculated precipitation vertical gradients is similar to that from previous studies (Guo et al., 2016; Cuo and Zhang, 2017). Previous studies revealed that precipitation vertical gradients during the wet season (May–September) ranged from −1.9 to 26.1 mm/100 m over the TP. The gradients in our study (−0.82 to 13.5 mm/100 m) are within this range. The differences in values may reflect that previous studies only considered the effects of elevation on precipitation (Guo et al., 2016; Cuo and Zhang, 2017).

3.2.3. GCM data and downscaling

The latest generation of GCMs from the Coupled Model Intercomparison Project Phase 5 (CMIP5) was used as climate change forcing data for our hydrological model. The performance of GCMs is not uniformly consistent within a given large geographical region due to differences in parameterization and physical processes (Miao et al., 2012; Liu et al., 2015b). We selected nineteen GCMs with better performance over the TP based on previous studies (Li et al., 2014; Su et al., 2013; Hu et al., 2014) and analyzed the mean projected changes in annual air temperature and precipitation between 1971–2006 and 2041–2070 from these GCMs for the RCP2.6 and RCP4.5 scenarios (not shown). Then, five GCMs that were closest to the mean value were selected for our studies (Table 4). The daily historical and future temperature, precipitation, and wind speed simulations of the five GCMs were obtained from the Centre for Environmental Data Analysis. However, the spatial resolutions of the GCMs outputs were too coarse to directly drive the hydrological model, thus requiring them to be downscaled.

The DC-V method (Bouwer et al., 2004; Immerzeel et al., 2012) is a statistically downscaled method in which the GCM data are corrected not only against the average observed climate but also for the observed variance. In this study, the DC-V statistically downscaled method was adopted to yield the daily future meteorological data for each meteorological station based on the historical station observations and simulations of GCMs during the baseline period (1971–2005). The future monthly values for each meteorological station from 2011 to 2100 were first calculated from the simulated value of GCM according to the following equation:

$$\alpha'_{station,m} = (\alpha_{gcm,m} - \alpha_{\bar{gcm},m}) \cdot \sigma_{obs,m}/\sigma_{gcm,m} + \alpha_{\bar{obs},m} \quad (10)$$

Table 3
Summary of the calculated precipitation gradient in response to elevation (Palt: mm/100 m), latitude (Plat: mm/°) and longitude (Plon: mm/°) for the five upstream river basins on the TP.

Drainage	Precipitation gradient	January	February	March	April	May	June	July	August	September	October	November	December
UYE	P_{alt}	0.086	0.179	0.288	0.099	0.756	1.041	2.306	0.737	0.470	−0.187	−0.069	0.002
	P_{lat}	−1.402	−1.919	−3.220	−6.640	−8.596	−19.200	−7.640	−13.022	−18.782	−14.049	−2.473	−1.098
	P_{lon}	0.049	0.496	1.342	2.998	8.682	3.990	11.695	7.601	6.501	3.264	0.286	−0.229
UYA	P_{alt}	0.498	0.426	0.500	0.687	0.199	1.861	0.991	0.669	0.367	0.926	0.356	0.269
	P_{lat}	0.927	0.971	2.124	2.999	6.982	8.882	5.322	5.915	6.918	3.926	0.805	0.576
	P_{lon}	−1.473	−1.173	−0.652	−2.058	−0.754	−12.068	−1.740	0.712	−2.831	−7.432	−0.836	−0.475
UM	P_{alt}	0.317	0.657	1.126	2.080	0.892	3.090	3.888	4.703	1.904	1.179	0.840	0.137
	P_{lat}	0.916	−0.824	−3.358	−8.262	2.832	0.071	−11.733	−17.730	−5.763	−5.876	−2.774	−0.105
	P_{lon}	−1.042	0.043	2.065	5.258	−1.558	−6.010	0.805	5.464	−1.724	2.124	1.306	−0.575
US	P_{alt}	0.076	0.625	1.290	2.486	2.307	2.399	3.263	2.958	2.300	0.297	0.587	0.066
	P_{lat}	−0.259	−2.151	−5.707	−9.591	−7.809	−0.255	−2.774	−6.186	−4.428	−0.385	−2.299	−0.708
	P_{lon}	0.105	1.677	3.884	6.919	6.633	7.203	4.490	3.968	5.421	5.389	1.787	0.111
UB	P_{alt}	0.483	0.867	0.747	−0.057	0.581	0.084	0.147	−0.323	−1.306	−0.554	0.532	0.332
	P_{lat}	−1.017	−4.668	−5.363	−1.812	5.299	24.970	−3.080	6.981	29.926	7.433	−0.440	−0.092
	P_{lon}	1.148	2.814	5.200	7.572	10.661	9.163	3.495	−2.619	4.414	5.340	1.634	0.749

where $\alpha'_{station,m}$ is the future corrected climate parameter (total precipitation or average temperature) in a particular month (m) for each meteorological station; $\alpha_{gcm,m}$ is the uncorrected simulated climate parameter from GCM; $\bar{\alpha}_{gcm,m}$ and $\sigma_{gcm,m}$ are the average and standard deviation of the simulated climate parameter over the baseline period, respectively; and $\bar{\alpha}_{obs,m}$ and $\sigma_{obs,m}$ are the average and standard deviation of the observed climate parameter over the baseline period, respectively.

The monthly future climate data of each meteorological station were subsequently disaggregated into daily values using the distribution of the daily output of the GCM from 2011 to 2100 and Eq. (11):

$$\alpha'_{station,d} = \begin{cases} \alpha_{gcm,d} \cdot \alpha'_{station,m} / \alpha_{gcm,m} & \text{for precipitation and windspeed} \\ \alpha_{gcm,d} + (\alpha'_{station,m} - \alpha_{gcm,m}) & \text{forairtemperature} \end{cases} \tag{11}$$

where $\alpha'_{station,d}$ is the future daily climate parameter of each meteorological station; $\alpha_{gcm,d}$ is the daily simulated climate parameter of GCM; and the subscript d represents the day.

The daily future climate parameters (temperature, precipitation, and wind speed) of the meteorological stations were interpolated into each model calculated cell to form the model forcing data according to the above interpolating algorithms.

3.2.4. Other data

The land surface data and parameters are also required by the VIC-CAS model, including soil parameters (e.g., soil field capacity, saturated hydrologic conductivity, and bulk density), land-use data (e.g., vegetation types, monthly albedo, and leaf area index), and topography.

The soil parameters were derived from the international Geosphere-Biosphere Program Data and Information System (IGBP-DIS), which contains global data for soil properties and global maps of soil distributions (Global Soil Data Task, 2014). The vegetation types and parameters were obtained from a 1 km global land cover map provided by the University of Maryland (Hansen et al., 2000). The topography data for our study catchments were obtained from Advanced Spaceborne Thermal Emission and Reflection Radiometer Global Digital Elevation Model Version 2 (ASTER GDEM V2, resolution: 10-arc-second), which was used to classify the snow/glacier elevation bands and digital river network.

Monthly observed streamflow data at control stations of the selected study basins (see Table 2 for data periods) were collected from the Qinghai and Tibetan Hydrological Bureau. These discharge data were utilized to calibrate and validate the model.

3.3. Model calibration and assessment criteria

The VIC-CAS model was calibrated against the updated glacier distribution of the SCGI and observed monthly discharge following a 2-step procedure: (I) glacier simulation calibration and (II) runoff generation calibration.

In this study, all glaciers of each catchment were divided into four size classes: < 1 km^2, 1–5 km^2, 5–10 km^2, and > 10 km^2. Model calibration and validation were conducted in each glacier size class. We used glacier data from the FCGI as the starting point of the simulation. The glacier data from SCGI were randomly separated into two parts in each size class: half was used for model parameters ($DDF_{snow/ice}$, R_{exp}) calibration, and the other half was used for model validation in each catchment. The $DDF_{snow/ice}$ and R_{exp} were calibrated to minimize the objective function Obj_g (Li et al., 2014; Liu et al., 2015b):

$$Obj_g = (1 - NS_g) + 5 \times |ln(1 + Er_g)|^2 \tag{12}$$

$$NS_g = \sum_{i=1}^{4} \left(\frac{A_i}{At} \times NS_{g,i} \right) \tag{13}$$

$$Er_g = \sum_{i=1}^{4} \left(\frac{A_i}{At} \times Er_{g,i} \right) \tag{14}$$

where $NS_{g,i}$ and $Er_{g,i}$ are the Nash-Sutcliffe efficiency and relative bias

Table 4
List of the global climate models used in this research.

Code	Model name	Country	Origination group(s)	Resolution
1	CSIRO-MK3.6.0	Australia	Commonwealth Scientific and Industrial Research Organization in collaboration with Queensland Climate Change Centre of Excellence	1.9° × 1.9°
2	HadGEM2-ES	Britain	Met Office Hadley Centre	1.2° × 1.9°
3	MIROC5	Japan	Atmosphere and Ocean Research Institute (The University of Tokyo), National Institute for Environmental Studies, and Japan Agency for Marine-Earth Science and Technology	1.4° × 1.4°
4	MIROC-ESM	Japan	Japan Agency for Marine-Earth Science and Technology, Atmosphere and Ocean Research Institute (The University of	2.8° × 2.8°
5	MIROC-ESM-CHEM	Japan	Tokyo), and National Institute for Environmental Studies	2.8° × 2.8°

Table 5
Main model parameter values for the five upstream river basins on the TP.

Basin	b	Ds	Ds_{max}	Ws	d_2	DDF_{snow}	DDF_{ice}	R_{exp}
UYE	0.25	0.1	11.0	0.6	0.3	4.8	8.1	0.4
UYA	0.10	0.1	10.0	0.8	1.0	4.3	7.2	0.4
UM	0.10	0.1	6.0	0.7	1.0	5.7	12.5	0.3
US	0.20	0.1	6.5	0.6	0.5	5.4	9.1	0.3
UB	0.10	0.1	6.0	0.7	0.6	4.5	7.9	0.4

(%) between simulated and observed glacier area for *ith* size class, respectively; A_i is the total glaciers area from FCGI within *ith* size class; A_t is total area of all glaciers in the study catchment; and NS_g and Er_g are the area-weighted average Nash-Sutcliffe efficiency and relative bias (%) of four glacier size classes, respectively.

In the second stage, the key soil parameters related to runoff (i.e., variable infiltration curve parameter b, thickness of the three soil layers (d_1, d_2, d_3), and parameters related to baseflow (Ds, Ds_{max} and Ws)) were calibrated against the observed monthly discharges from 1980 to 1985 for the US and from 1971 to 1990 for others based on data availability. A similar objective function (Obj_r) that is minimized during calibration was used as follows:

$$Obj_r = (1 - NS_r) + 5 \times |ln(1 + Er_r)|^2 \quad (15)$$

where NS_r and Er_r are the Nash-Sutcliffe efficiency and relative bias (%) between simulated and observed streamflow, respectively.

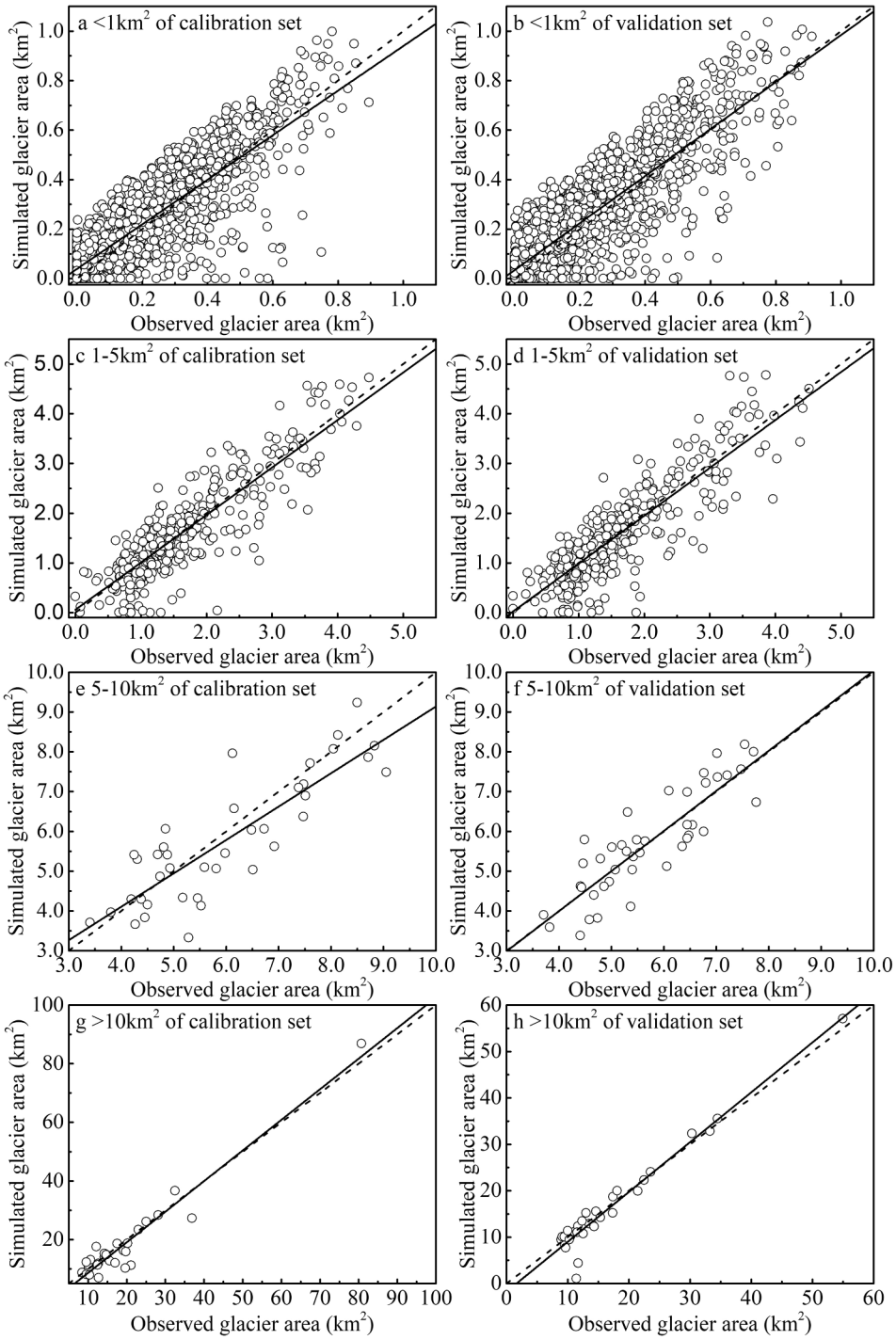

Fig. 4. Comparisons between simulated and observed glacier areas at < 1, 1–5, 5–10, and > 10 km² classes of calibration and validation sets for the five major upstream river basins on the TP.

Table 6
Model performance for simulating glacier area evolution.

	Calibration set					Validation set				
	$< 1\,km^2$	1–5 km^2	5–10 km^2	$> 10\,km^2$	*AWA*	$< 1\,km^2$	1–5 km^2	5–10 km^2	$> 10\,km^2$	*AWA*
NS	0.69	0.73	0.69	0.91	0.77	0.71	0.69	0.67	0.93	0.76
R^2	0.74	0.77	0.73	0.93	0.81	0.77	0.75	0.76	0.95	0.81
Er	15.0%	−1.0%	−3.6%	−5.3%	0.4%	16.7%	−2.3%	0.1%	−3.1%	1.7%

AWA is the area weighted average value of four glacier size calsses.

The Nash-Sutcliffe efficiency (*NS*) and relative bias (*Er*) are defined as follows::

$$NS = 1 - \sum_{i=1}^{n} (Q_{obs,i} - Q_{sim,i})^2 / \sum_{i=1}^{n} (Q_{obs,i} - \bar{Q}_{obs})^2 \quad (16)$$

$$Er = 100 \times \left(\sum_{i=1}^{n} Q_{sim,i} - \sum_{i=1}^{n} Q_{obs,i} \right) / \sum_{i=1}^{n} Q_{obs,i} \quad (17)$$

where $Q_{obs,i}$ and $Q_{sim,i}$ are the observed and simulated discharges or glacier area at the *ith* month or glacier, respectively; and $\bar{Q}_{obs}$ and $\bar{Q}_{sim}$ are the mean of the *n* observed and simulated values, respectively. The coefficient of determination (R^2) was also used to assess the model performance:

$$R^2 = \left[\sum_{i=1}^{n} (Q_{obs,i} - \bar{Q}_{obs})(Q_{sim,i} - \bar{Q}_{sim}) \right]^2 / \sum_{i=1}^{n} (Q_{obs,i} - \bar{Q}_{obs})^2 \sum_{i=1}^{n} (Q_{sim,i} - \bar{Q}_{sim})^2 \quad (18)$$

4. Results

In this section, we assess the model performance for runoff and glacier area change based on historical observations. We also project future runoff and glacier area changes using the VIC-CAS model forced by the downscaled outputs of GCMs under two emission scenarios (RCP2.6 and RCP4.5). We further compare our projected results with previous studies and discuss the uncertainties.

4.1. VIC-CAS model performance

In our study, to accurately estimate glacier and snow melt, the glaciers were split into a number of glacier elevation bands with 100-m intervals, while ice-free land was divided into six snow elevation bands in each calculated unit. To achieve a full modeling spin-up, the simulated period was started in 1961, and the simulated results after 1971 were used to calibrate and validate the model. The VIC-CAS model was successfully calibrated to reproduce the observed glacier area and monthly streamflow. The values of the optimized parameters are presented in Table 5.

Comparisons between the simulated and observed glacier area from the SCGI for calibration and validation sets during the same time period are shown in Fig. 4. The model achieved reasonably satisfactory results in terms of the mean *NS*, R^2 and *Er*, which were 0.77, 0.81 and 0.4% for the calibration set and 0.76, 0.81 and 1.7% for the validation set, respectively (Table 6). The model overestimated the area of small glaciers ($< 1\,km^2$) with a larger relative bias (15.1% and 16.7% for the calibration and validation periods, respectively) but underestimated the area of larger glaciers with a smaller relative bias. This phenomenon might be a consequence of the parameters of the glacier volume-area scaling law, which were obtained from the observations of worldwide glaciers with sizes ranging from 0.1 km^2 to 1000 km^2 (Grinsted, 2013). Previous studies (Bahr et al., 2009; Bahr, 2011) have suggested that the estimated total volume from many glaciers is more accurate and the simulation accuracy depends on the amount of sampling data as well as sampling biases, such as preferentially choosing larger glaciers over smaller glaciers. In our study, errors that overestimated small glaciers were offset by errors that underestimated large glaciers; therefore, the simulated error for the total area of glaciers was very low (*Er* < 2%) in our study catchment.

Fig. 5 shows the multi-year average monthly observed and simulated discharge, and Table 7 summarizes the model performance for the five study catchments. The model shows reasonably satisfactory simulated discharge, with *NS* ranging from 0.82 to 0.94, R^2 ranging from 0.82 to 0.94, and *Er* ranging from −0.3% to −5.4% during the calibration period. The calibrated model reproduced the observed streamflow satisfactorily during the validation period, as indicated by the high mean *NS* and R^2 and the low mean *Er* values of 0.86, 0.87, and 1.7%, respectively.

Hence, the VIC-CAS model is able to realistically simulate the glacier area change and discharge with relatively high accuracy given the large scale, data scarcity, heterogeneity, and complexity of the five major upstream river basins on the TP.

4.2. Evaluation of the downscaling method

In this study, the DC-V statistical downscaling method (Bouwer et al., 2004; Immerzeel et al., 2012) was applied to bias-correct raw GCM meteorological elements at the closest grid point to a given station so that climatological distribution of meteorological elements matched the observed distribution. Precipitation is the most important driver in hydrological models. Fig. 6a–d compares the annual total precipitation time series and mean monthly precipitation of the raw GCM outputs, bias-corrected GCM results and meteorological station observations over 1980–2005, during which all stations have a continuous record. The raw GCM results did not reproduce the observed pattern of the monthly cycle and significantly overestimated the magnitude of precipitation (Fig. 6a and b). After bias-correction, the accuracy of monthly mean precipitation was significantly improved (Fig. 6d). Note that the bias-corrected annual results are not expected to reproduce the actual annual time series (Fig. 6c) since the GCMs did not use actual boundary conditions in the simulations (Hwang and Graham, 2013).

To further evaluate the performance of the downscaling method, a comparison was performed between the observed and simulated runoff using bias-corrected GCM data from 1971 to 1999 in the UB, and the results are shown in Fig. 6e, f. The simulated results using bias-corrected data exactly reproduced the observed mean monthly runoff with *Er* ranging from −0.4% to −6.2% (Fig. 6f). The observed annual time series of runoff could not be reproduced by simulation (Fig. 6e). Overall, the DC-V downscaling method is feasible for bias-correcting the raw GCM output for hydrological simulation and projection.

4.3. Historical and future climate change

Over the previous 40 years, the annual average air temperature has shown a significant increasing trend in all five catchments. The annual average air temperature across the entire study region has increased at an average rate of 0.42 °C per decade. The model projections indicate that warming will continue through the late 21st century. As expected, Scenario RCP4.5 is generally warmer than Scenario RCP2.6. For all study basins (Fig. 7), the multi-model mean projects that the annual average temperature will increase by 2.0 (2.5)°C in the 2050 s

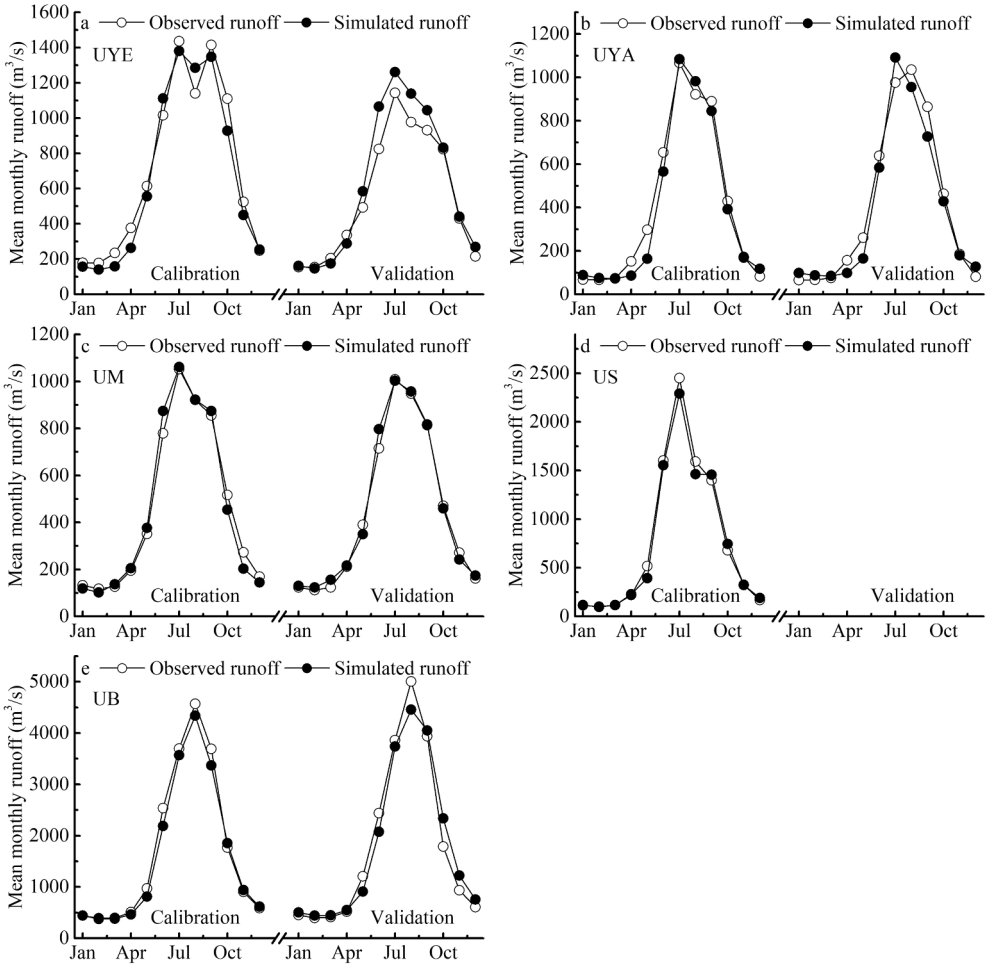

Fig. 5. Average observed and simulated annual hydrographs during the calibration and validation periods for the upstream region of five major river basins on the TP.

(2051–2060) and 1.9 (3.2)°C in the 2090 s (2091–2100) in comparison to 1971–2010 under the RCP2.6 (RCP4.5) global emissions scenarios. These values are equivalent to approximately 0.11 °C (for RCP2.6) and 0.31 °C (for RCP4.5) of warming per decade.

The precipitation showed different patterns for the five major upstream river basins over the past several decades due to different moisture sources. Overall, the precipitation showed a non-apparent increasing trend except for the UYE. The annual precipitation showed increasing trends of 11.6, 12.1, 17.2, and 22.4 mm per decade in the UYA, UM, US, and UB, respectively. However, a decreasing trend of −1.7 mm per decade was found for the precipitation in the UYE (Fig. 7). The averages of the five GCMs under RCP2.6 and RCP4.5 for the 2050 s and 2090 s suggested that the five study catchments will experience an increasing annual precipitation (Fig. 6). The mean precipitation across the five catchments is projected to increase by 6.6 (14.3) mm per decade under RCP2.6 (RCP4.5) emission scenarios. Compared to the baseline of 1971–2010, the multi-model average annual precipitation is projected to increase by 12.1–25.3 (13.1–25.4)% in the 2050 s and 13.5–23.4 (19.9–40.9)% in the 2090 s for the five major upstream river basins under RCP2.6 (RCP4.5) emission scenarios.

4.4. Hydrology responses to climate changes

4.4.1. Fate of glaciers

The glacier area revealed a significant decreasing trend in the UYE (−20.3%), UYA (−15.6%), UM (−34.4%), US (−37.3%), and UB (−32.7%) over the past 40 years. In general, the glaciers shrank more rapidly in the western catchments of the TP. The mean values of glacier area loss in the studied catchments (UYE, UYA, UM, US, and UB) under RCP2.6 (RCP4.5) between 2010 and 2060 were determined to be 39.6

Table 7
Model performance for simulating monthly runoff.

Basin	Calibration period					Validation Period				
	NS	R^2	*Er*	*OMMR*	*SMMR*	*NS*	R^2	*Er*	*OMMR*	*SMMR*
UYE	0.82	0.82	−5.2%	705.84	669.20	0.78	0.81	10.7%	557.24	617.11
UYA	0.88	0.89	−4.8%	406.24	386.76	0.87	0.87	−5.1%	405.96	385.44
UM	0.90	0.90	−0.3%	457.12	455.98	0.89	0.89	1.4%	445.57	451.92
US	0.92	0.93	−3.4%	773.76	747.78	–	–	–	–	–
UB	0.94	0.94	−5.4%	1704.44	1612.53	0.92	0.92	−0.4%	1796.94	1790.46

OMMR and *SMMR* are the observed and simulated mean monthly runoff (m^2/s), respectively.

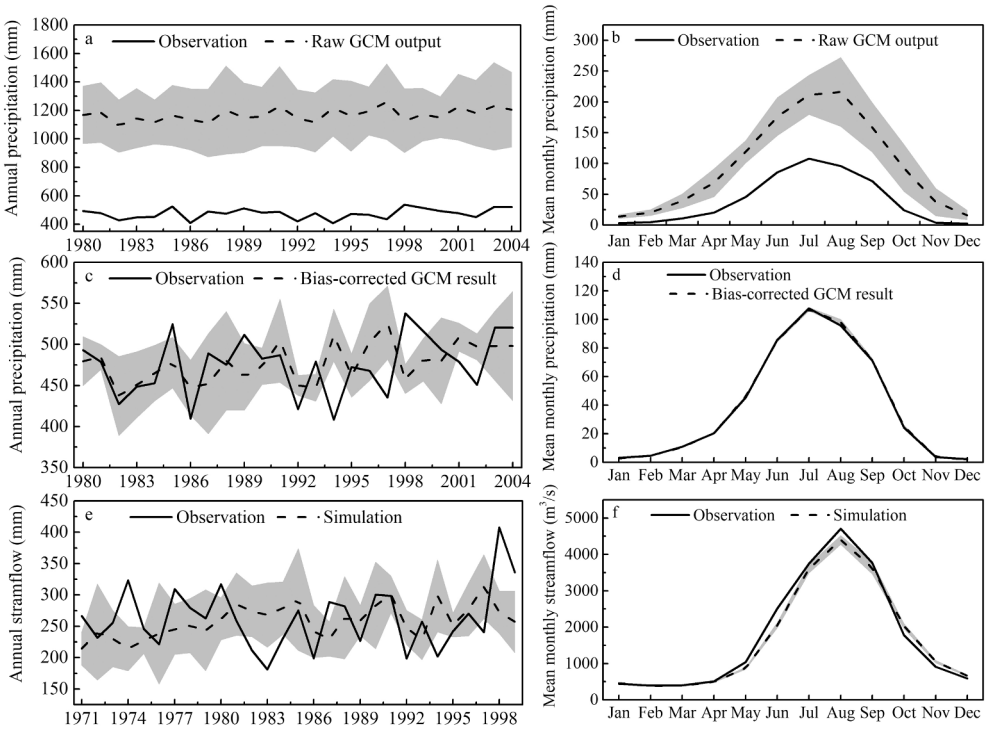

Fig. 6. (a–d) Comparison of the average annual total precipitation time series and the mean monthly precipitation for the raw GCM outputs, bias-corrected GCM results and observation of meteorological stations. (e, f) Comparison of the annual and mean monthly streamflow for observation and simulation using the bias-corrected GCM results in the UB. The solid dashed line represents the ensemble means, and the gray envelope represents the bounds of the results from 5 GCMs.

(45.6)%, 53.8 (57.6)%, 82.5 (84.8)%, 67.2 (69.9)%, and 52.3 (58.3)%, respectively (Fig. 8), and by the end of the 21st century, the glacier area is projected to decline by 46.6 (62.1)%, 70.8 (80.9)%, 88.2 (95.6)%, 71.8 (79.6)%, and 60.0 (75.8)% in the five catchments, respectively. The glacier retreat during the first half of the 21st century will be much faster than that during the latter half of the 21st century. The glaciers are located at a higher altitude region during the latter half of the 21st century due to former shrinkage; therefore, the glacier area change is less sensitive to climate change. In addition, the annual mean air temperature is projected to reach a peak in the 2050 s under the RCP2.6 emission scenario (Fig. 7).

4.4.2. Stream flow projections

Fig. 9 displays the runoff projections with the five downscaled GCMs. According to the runoff separation results, the total runoff depends marginally on the glacier melt in the UYE (0.35%), UYA (3.7%),

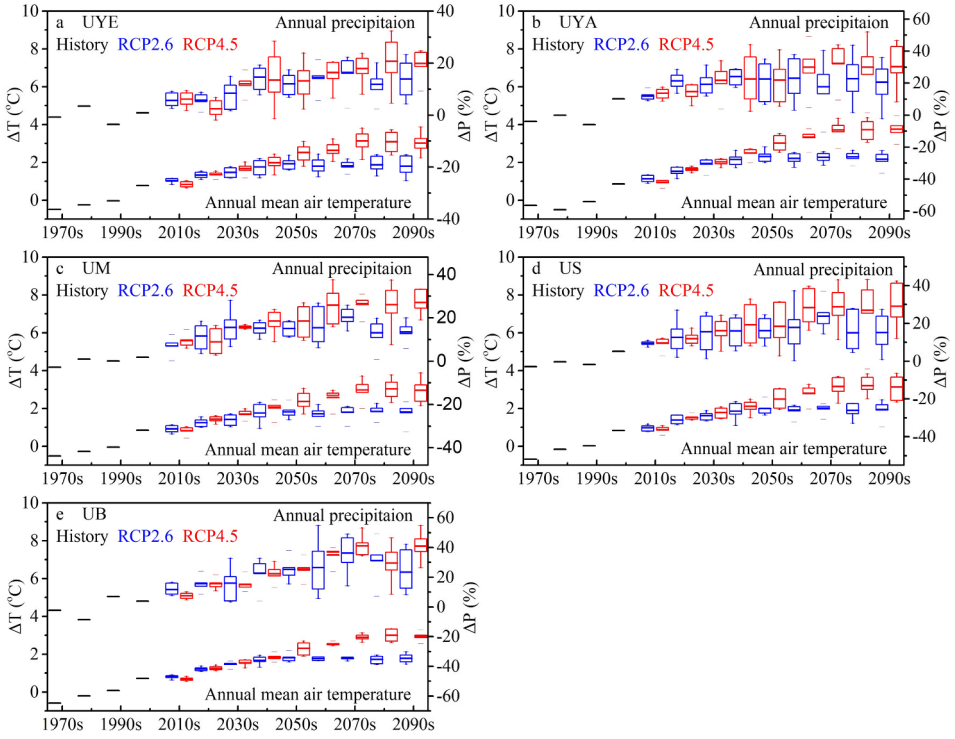

Fig. 7. Historical and future climate change relative to the mean value of the baseline time period (1971–2010) for the five major upstream river basins on the TP. In the box-and-whisker plots, the centerlines show the mean, box limits indicate the 25th and 75th percentiles, and whiskers denote minimum and maximum values.

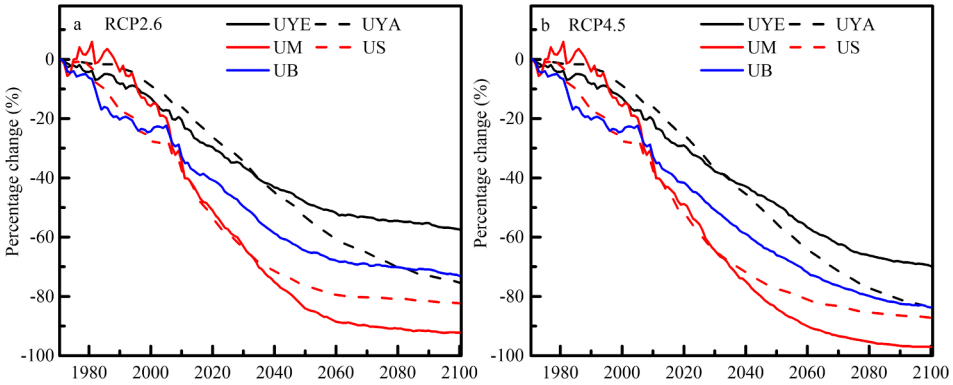

Fig. 8. Simulated percentage change in glacier area relative to 1971 for the five major upstream river basins on the TP.

UM (1.3%), US (4.4%), and UB (5.5%) due to limited glacier coverage (Fig. 8 and Table 2). Our study shows that glacier runoff will increase in the UYA at least until the 2020 s (2021–2030) and will begin to decrease after the 2030 s (2031–2040) (Fig. 9). However, glacier runoff in the UYE, UM, US, and UB had exceeded its tipping point at the beginning of the 21st century, and more than 20% of glacier area loss occurred from 1971 to 2010. When the increasing melt rate due to higher air temperatures cannot compensate for the negative effect of glacier area loss on melt water, glacier runoff will start to decline. The multi-model median results show that glacier runoff in the 2050 s will decline by 37.5 (26.1)%, 19.8 (16.9)%, 80.3 (79.6)%, 69.1 (67.7)%, and 48.9 (46.0)% compared with the historical reference period (1971–2100) for the five catchments (UYE, UYA, UM, US, and UB, respectively) under the RCP2.6 (RCP4.5) global emission scenarios. By the end of the century (2090 s), the glacier runoff is predicted to decrease within each basin by up to 51.3 (61.3)%, 62.2 (65.4)%, 91.0 (95.7)%, 77.2 (80.1)%, and 59.1 (71.6)% compared with the reference period, respectively.

Snowmelt runoff is an important component of the total runoff. The historical simulation showed that the contribution of snowmelt runoff to the total runoff was 15.3%, 12.2%, 28.8%, 28.3%, and 23.1% for the UYE, UYA, UM, US, and UB, respectively. The snowmelt runoff is projected to increase in the five catchments until the 2020 s and to start to decrease after the 2030 s, potentially owing to a decrease in the snowfall due to smaller snow/precipitation ratio with the warming climate (Fig. 9).

In comparison to 1971–2010, a consistent increase in total runoff is projected for all the basins in the two periods (2050 s and 2090 s), for which the increasing rainfall runoff that compensates for the loss of snow/ice melt water is the major cause. The total runoff in the 2050 s is projected to increase by 7.1 (6.5)% for the UYE, 26.4 (12.2)% for the UYA, 19.7 (21.1)% for the UM, 11.8 (12.6)% for the US, and 21.8 (16.8)% for the UB under the RCP2.6 (RCP4.5) emission scenarios. By the end of the 21st century (2090 s), the total runoff will increase by 8.8 (11.9)%, 19.2 (14.0)%, 15.8 (32.4)%, 9.9 (21.5)%, and 16.9 (30.7)% in the five respective basins (same order as previous sentence) for the RCP2.6 (RCP4.5) emission scenarios, respectively.

4.4.3. Seasonality of future runoff

The seasonal cycle changes for each simulated runoff component from historical records and future predictions are shown in Fig. 10. By the end of this century, the contribution of glacier runoff to total runoff will be negligible due to a large decrease in glacier area (Figs. 8 and 10). Positive snowmelt runoff changes are projected during the spring (March-May) and late autumn (October-November) for the UYE, UYA, US, and UB, indicating an earlier spring snow melt and delayed fall freeze-up. Obvious negative snowmelt changes are observed during the summer (June-August) for the five major upstream river basins, which can be explained by decreased precipitation in the form of snowfall with the warming climate. The rainfall runoff is predicted to increase during May-June because of the increasing rainfall/precipitation ratio.

The pattern of runoff is similar to that of precipitation for the five basins, with 60–80% of the annual streamflow occurring from June-September. The annual hydrograph remains practically unchanged except for the UYE, where the total runoff peak is anticipated to occur 1 month earlier (July–June). The shift can be explained by an earlier onset of spring snowmelt and an increase in the rainfall/precipitation ratio in May–June (Fig. 10b and c). The large positive total runoff changes are generally projected during the cold season (January–March and November–December) for the five major basins. Additionally, the increased total runoff in the cold season is a major cause of the increase in total runoff. The increasing rate of warm season (May–October) streamflow was clearly less than that of the annual and cold seasons, and a negative trend in warm season streamflow was even found with a slight increase in annual streamflow in the UYE and UYA (Fig. 10 and Table 8). The differences in streamflow change in the warm and cold season were most likely related to the degradation of permafrost soil, which results in an increased infiltration during the warm season and greater water release during the cold season.

5. Discussion

5.1. Comparison with other models

Water resource management of glacierized catchments largely relies on glacio-hydrological models that can estimate glacier meltwater contribution to streamflow and project future streamflow change. However, few current macroscale watershed models incorporate glacier modeling in macroscale applications (Radić and Hock, 2014). Several studies have tried to couple the temperature-index (Immerzeel et al., 2010; Luo et al., 2013; Zhang et al., 2013; Zhao et al., 2015; Su et al., 2016) or energy-balance (Kotlarski et al., 2010; Zhao et al., 2013) glacier melt model to existing macroscale hydrological models, such as the VIC model, Soil and Water Assessment Tool (SWAT) and Snowmelt Runoff Model (SRM). Although the energy-balance melt method more properly describes the physical processes determining melt, the temperature-index method is the most widely used approach to simulate snow/ice melt. The temperature-index method often achieves better model performance than the energy-balance method at the catchment scale because temperature is the least uncertain available climate variable (Hock, 2003, 2005; Essery et al., 2013; Pellicciotti et al., 2013). Hence, the temperature-index method is most common and will retain its foremost position in snow/ice melt estimating due to low data requirements and good performance. In this study, the extended degree-day method considering the impact of the surface aspect on melt was coupled to VIC model.

For both the current climate and future climate scenarios, simulations of glacier area evolution are indispensable. Few studies at the

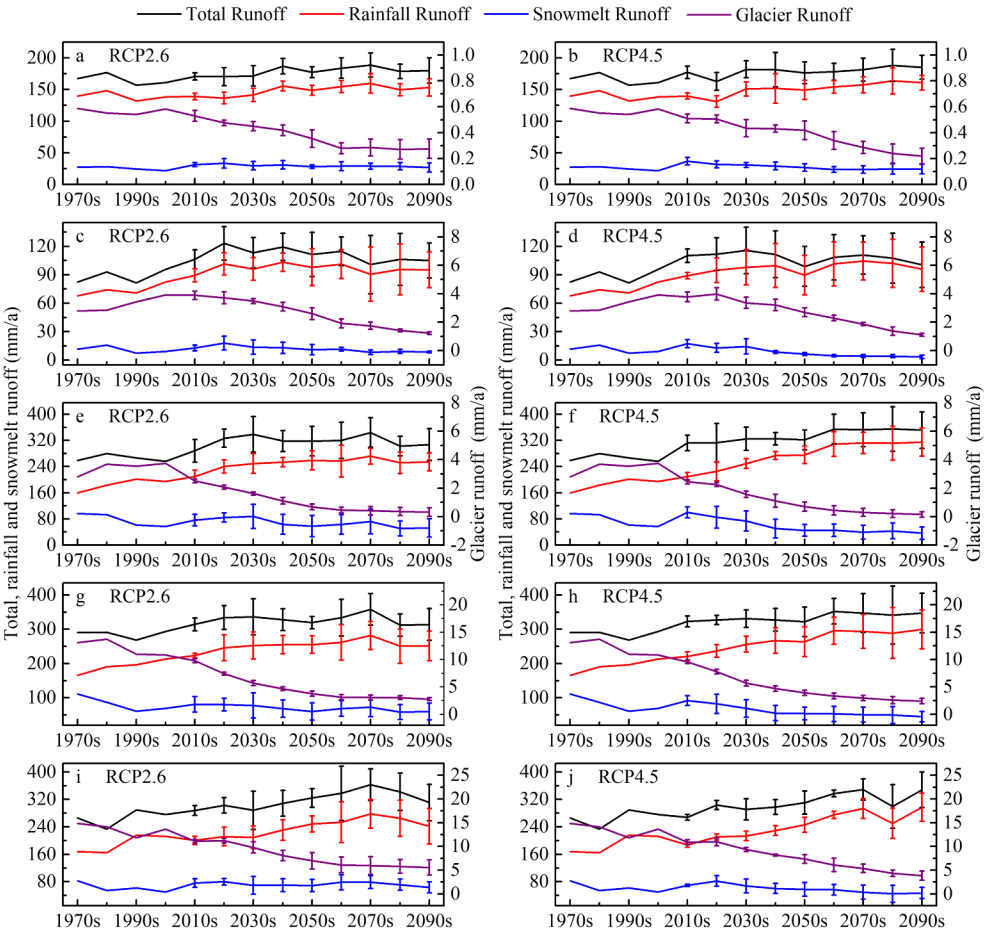

Fig. 9. Mean of all catchment runoff simulations for each decade, RCP, and study area (a and b: UYE; c and d: UYA; e and f: UM; g and h: US; i and j: UB). The error bars represent the standard deviations of the mean.

local scales have incorporated simple area evolution schemes (volume-area scaling approach) into hydrological models (Stahl et al., 2008; Luo et al., 2013; Lutz et al., 2014; Su et al., 2016). Most previous studies (Luo et al., 2013; Lutz et al., 2014; Su et al., 2016; Zhao et al., 2013, 2015) consider all glaciers as whole to be simulated in a calculated unit and neglect the differences in mass balance and area change among different glaciers, especially for glaciers of different sizes. It is difficult to directly calibrate and validate models using glacier outlines derived from remote sensing data collected during several different time periods and the observed mass balance of individual glaciers, which is necessary to reduce the uncertainty in hydrological simulations of larger glacierized catchments (Stahl et al., 2008; Huss et al., 2008; Konz and Seibert, 2010; Duethmann et al., 2015; Immerzeel et al., 2012). The VIC-CAS model presented here attempts to incorporate these advances. The model includes a representation of individual glaciers on the sub-basin scale and simulates mass balance and area evolution for an individual glacier.

5.2. Necessity of model calibration using glacier change data

Most recent studies suggest that the main driver of future runoff change is the change in precipitation in the upstream regions of large river systems on the TP, which is consistent with our findings (Table 1). However, there is debate about the contributions and future trends of glacier melt water across three previous studies (Immerzeel et al., 2010; Lutz et al., 2014; Su et al., 2016), which accounted for glacier hydrological processes using the degree-day method.

DDFs are key parameters in the degree-day melt model, and differences among *DDFs* lead to different simulated contributions and future trends of glacier melt water. However, there are significant differences in the values of *DDFs* (DDF_{snow} ranging from 4.0 to 4.8 mm °C day^{-1} and DDF_{ice} ranging from 7.0 to 13.8 mm °C day^{-1}) among the previous studies, which were obtained from limited observations of several glaciers (Su et al., 2016) and calibration by comparing the simulated streamflow with observed records (Immerzeel et al., 2010; Lutz et al., 2014). *DDFs* from these limited observations may not accurately represent the average conditions of the large-scale catchments because of the high spatial and temporal heterogeneities of *DDFs* (Ramanathan and Carmichael, 2008). Furthermore, it is difficult to obtain reliable *DDFs* through model calibration only based on streamflow due to inaccurate precipitation input.

Fig. 11 shows the VIC-CAS model sensitivity to the *DDF* parameters in terms of the objective function of evaluating the performance of streamflow simulation (Obj_r) and glacier runoff contribution during the calibration period. The Obj_r was less sensitive to *DDFs* than the glacier melt water contribution, with an approximate change of 0.03%, 0.14%, 0.03%, 0.58%, and 0.97% in Obj_r for every 10% change in *DDFs* for the UYE, UYA, UM, US and UB, respectively. A 10% increase in *DDFs* will increase the glacier runoff contribution to streamflow by 2.3%, 4.6%, 1.2%, 1.8%, and 1.6% for the five catchments, respectively. As shown in Fig. 11, the optimized value of *DDFs* calibrated only by in-situ observed streamflow was < 0.5 times $DDFs_0$ (the value of *DDFs* from the calibration by glacier area) for the UYE, 1.0 times $DDFs_0$ for the UYA, and > 1.5 times $DDFs_0$ for the UM, US, and UB. The differences

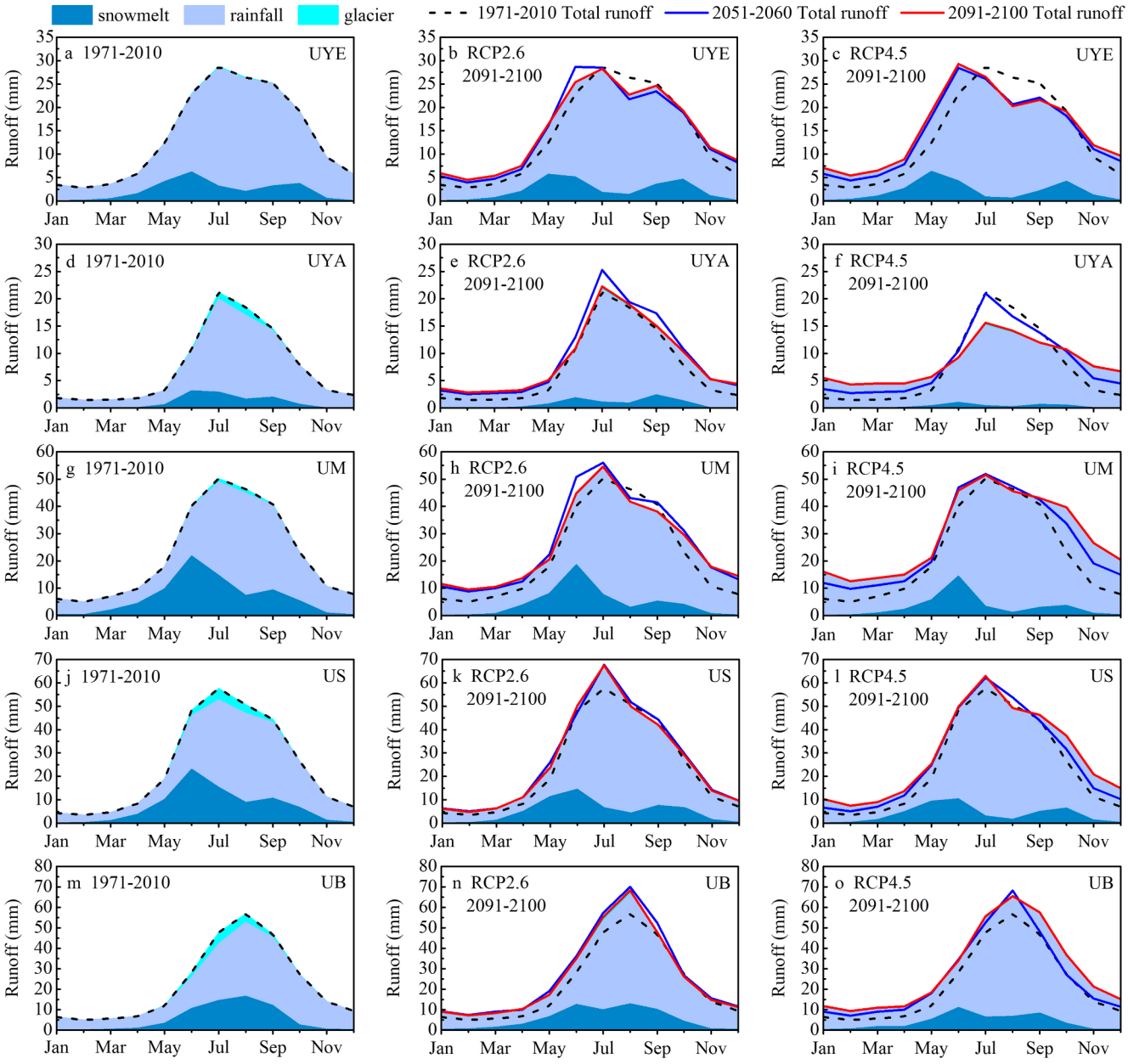

Fig. 10. Simulated seasonal runoff cycles and water input composition. The median results of all simulations are represented. The composition of water inputs is shown for the reference period (1971–2010) and for 2091–2100 under the RCP2.6 and RCP4.5 projections. Solid lines represent the mean of all simulated total runoff results for the reference period and two future periods (2051–2060 and 2091–2100).

Table 8
Change in future streamflow relative to baseline period (1971–2010).

Drainage	Scenario	2050 s (2051–2060)			2090 s (2091–2100)		
		Annual	Cold season	Warm season	Annual	Cold season	Warm season
UYE	RCP2.6	7.1%	29.9%	1.9%	8.8%	41.2%	1.4%
	RCP4.5	6.5%	39.4%	−1.0%	11.9%	60.5%	0.8%
UYA	RCP2.6	26.4%	71.6%	19.2%	19.2%	84.2%	8.8%
	RCP4.5	12.2%	81.1%	1.2%	14.0%	172.3%	−11.3%
UM	RCP2.6	19.7%	56.1%	11.9%	15.8%	66.7%	4.9%
	RCP4.5	21.1%	70.1%	10.6	32.4%	123.7%	12.9%
US	RCP2.6	11.8%	34.7%	8.1%	9.9%	32.4%	6.3%
	RCP4.5	12.6%	42.2%	7.9%	21.5%	94.3%	9.9%
UB	RCP2.6	21.8%	32.9%	19.5%	16.9%	29.3%	14.2%
	RCP4.5	16.8%	31.0%	13.7%	30.7%	69.0%	22.5%

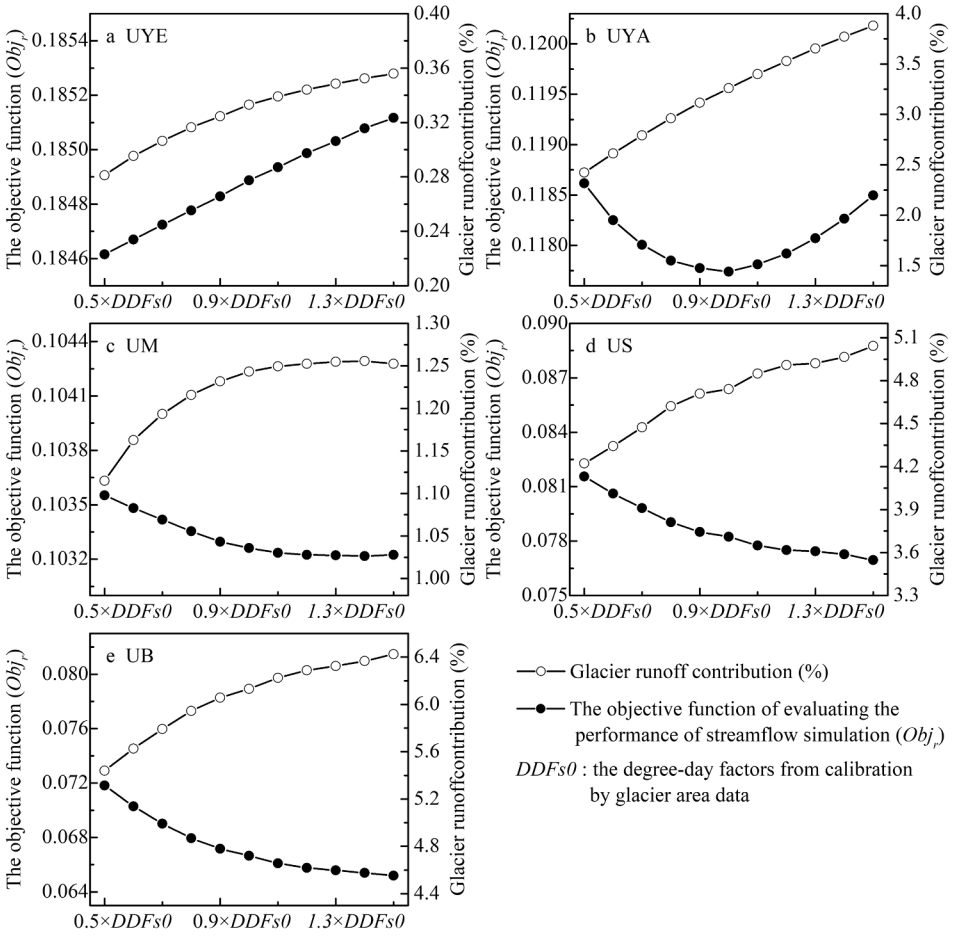

Fig. 11. Model sensitivity to the degree-day factors in terms of glacier runoff contribution and objective function of evaluating the performance of streamflow simulation (Obj_r) for the UYE, UYA, UM, US, and UB basins.

between optimized values of *DDFs* through in-situ observed streamflow and glacier area data were, excluding the UYA, greater than 50%.

The uncertainties in total runoff simulation from *DDFs* were minimal because of the limited glacier melt water contribution. In contrast, the uncertainties in the glacier area and glacier runoff simulations associated with *DDFs* were considerably larger. Fig. 12 illustrates the simulated and projected glacier area and glacier runoff change when *DDFs* increased or decreased by 50%. Increasing *DDFs* led to accelerated glacier area loss and decreased glacier meltwater in the 2050 s and 2090 s. The ranges of simulated glacier runoff and glacier area change informed by different *DDFs* (0.5 × *DDFs*, 1.0 × *DDFs*, and 1.5 × *DDFs*) were also found to be very large. A 50% change in degree-day factors caused 35.0–169.1 (37.1–172.5)% and 36.3–217.5 (43.1–332.2)% differences in glacier area and 30.6–146.9 (26.8–145.0)% and 34.4–223.0 (42.5–335.7)% differences in glacier runoff for the five study catchments in the 2050 s and 2090 s under the RCP2.6 (RCP4.5) emission scenario, respectively. Additionally, glacier runoff reached a tipping point 10–30 years earlier or later when the *DDFs* increased or decreased by 50%. Thus, observed glacier information must be used for model calibration to obtain more realistic *DDFs*. The complex topography and observed data scarcity on the TP substantially limit melt model calibration via glacier mass balance, which has usually been adopted in previous studies (Stahl et al., 2008; Huss et al., 2008; Konz and Seibert, 2010; Immerzeel et al., 2012; Duethmann et al., 2015). Remote sensing glacier area data represent valuable alternatives to ground-based observations for calibration on the TP because their spatially distributed patterns, spatial resolution, and availability are not significantly impacted by terrain.

5.3. Uncertainties in projections

Uncertainties in projections are attributable to the following: (1) different model parameters; and (2) the adopted global climate models, global emission scenarios and downscaling approaches (Huss et al., 2014; Chiew et al., 2010).

The uncertainties in runoff simulations of the same catchments in our study generated by the VIC hydrological model soil parameters have been discussed and analyzed by Zhang et al. (2013) and Su et al. (2016). Their studies indicated that the uncertainties associated with model soil parameters are much smaller than those from climate change projections. The uncertainties in the parameters (c and γ) of the volume-area scaling law, which is typically adopted to simulate glacier advance or retreat in a large-scale catchment, may represent an additional contribution (except *DDFs*) to uncertainties in glacier simulation. There are many empirical parameters of the volume-area scaling law (Grinsted, 2013). The parameters of the scaling law from Radić and Hock (2010) were used by Immerzeel et al. (2010), Lutz et al. (2014) and in our study, while the parameters from Liu et al. (2003) were adopted by Su et al. (2016). We also compared the glacier area and glacier runoff simulations by adopting four recognized volume-area scaling laws (Table 9). We found that Huss's scaling law shows a relatively poor performance for glacier area compared with the other three

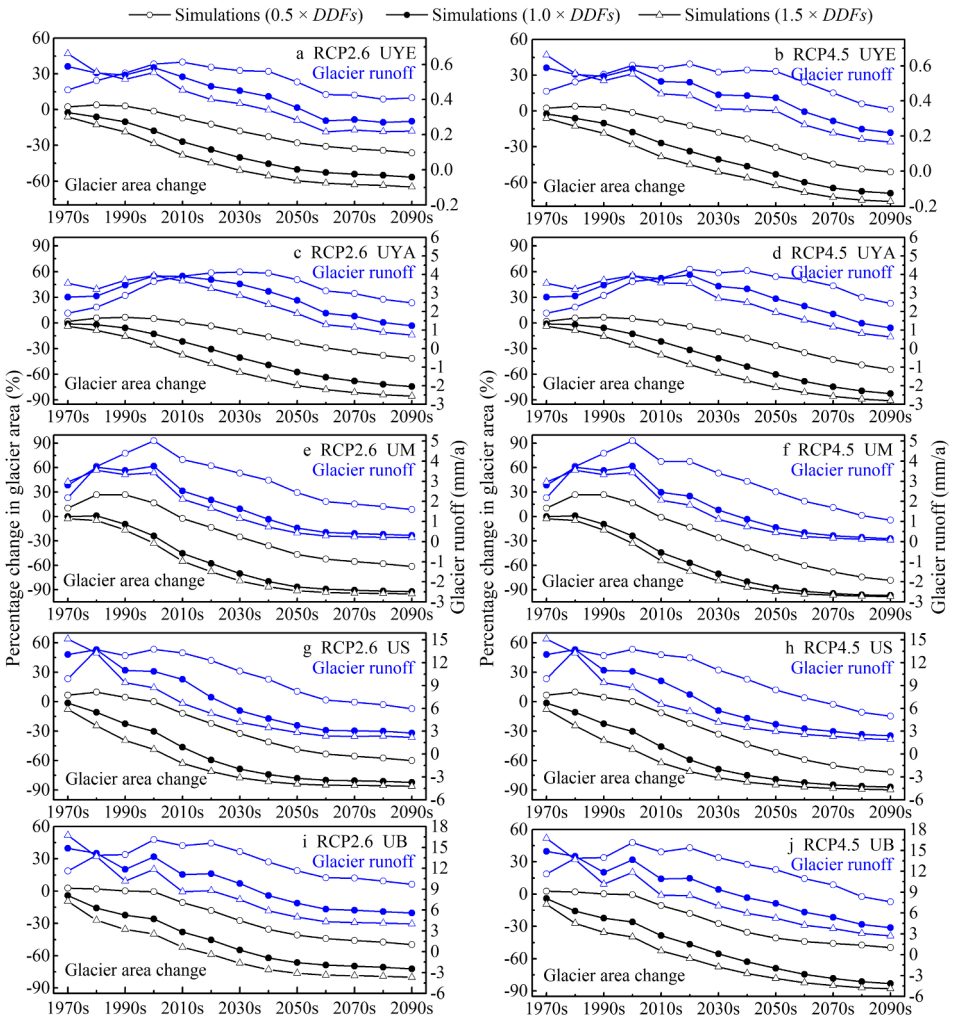

Fig. 12. Simulations of glacier runoff and percentage change in glacier area for the five upstream river basins on the TP using different degree day factors (0.5 × *DDFs*, 1.0 × *DDFs* and 1.5 × *DDFs*).

methods, which achieved a similarly effective model performance (not shown). Our results reveal that the uncertainties in simulations of glacier runoff and glacier area change from the four volume-area scaling laws are small, with mean uncertainties of less than 4.0% and 5.0%, respectively (Fig. 13). Additionally, there is almost no difference between the simulations that adopt Grinsted's, Radić's, and Liu's scaling laws. The uncertainties in *DDFs* are considered to be the major source of uncertainties in the glacier area and glacier melt water projections.

Generally, the spread in GCMs results accounts for the high percentage of overall uncertainty in the projected results (Teng et al., 2012; Immerzeel et al., 2013; Huss et al., 2014; Barria et al., 2015a,b; Peel et al., 2015). Although 5 GCMs with projections closest to the mean values of 19 GCMs were selected, the ranges in future annual precipitation and mean air temperature projections downscaled from the selected GCMs were found to be very large. The changes in projected mean annual precipitation range from 10.3 to 29.6 (8.3–32.9)% and 3.8 to 33.0 (16.2–43.2)%, and the temperature vary from 1.7 to 2.4 (2.0–3.1) °C and 1.2 to 2.4 (2.5–3.8) °C in comparison to the reference period for our study basins in the 2050 s and 2090sunder the RCP2.6 (RCP4.5) emission scenario, respectively (Fig. 6). The ranges of the projected annual total runoffs informed by the 5 GCMs were considerably large, with an average relative standard deviation (standard deviation divided by the mean) of 4.9 (9.9)% and 11.1 (10.1)% for the UYE, 21.0 (21.4)% and 17.6 (23.8)% for the UYA, 14.2 (9.4)% and 15.8 (15.9)% for the UM, 5.6 (13.3)% and 14.8 (16.7)% for the US, and 8.3 (10.8)% and 17.3 (15.0)% for the UB in the 2050 s and 2090 s under the RCP2.6 (RCP4.5) emission scenario, respectively (Fig. 9). The spread of future climate and runoff projected results was even larger for certain

Table 9
Recognized glacier volume-area scaling laws, as obtained from the literature.

References	Volume-Areascaling laws	Comments
Grinsted (2013)	$V = 0.0433 \cdot A^{1.290}$	Obtained from minimizing the absolute volume deviation from glacier inventory data
Radić and Hock(2010)	$V = 0.0365 \cdot A^{1.375}$	Based on earlier studies
Huss and Farinotti (2012)	$V = 0.0259 \cdot A^{1.275}$	Relationship for Central Asia
Liu et al. (2003)	$V = 0.0395 \cdot A^{1.350}$	From the observation of Qilian and Tien Shan

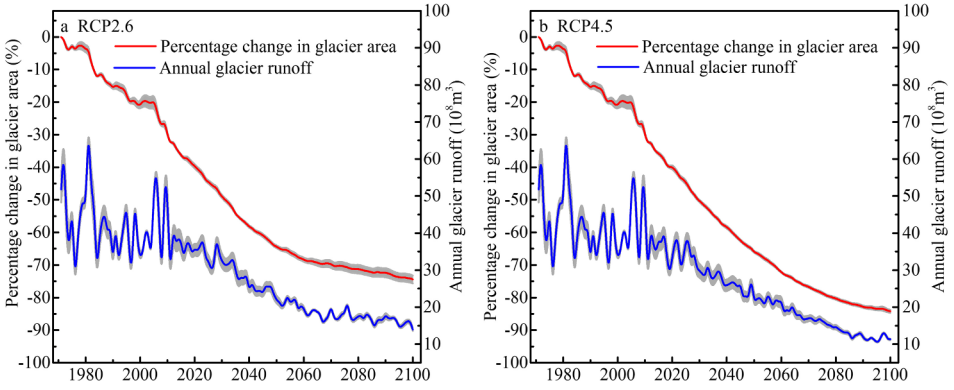

Fig. 13. Simulated results of total glacier runoff and percentage change in the glacier area of the five upstream river basins on the TP using Grinsted's, Radić's, Huss's and Liu's volume-area scaling laws. The solid line represents the ensemble means, and the gray swath represents the spans of results from the four volume-area scaling laws.

seasons. The uncertainties in glacier projections with different climate changes from the five GCMs were also very apparent, with an average relative standard deviation of 15.8 (14.0)% for glacier runoff and 13.0 (12.6)% for glacier area across our study catchments under the RCP2.6 (RCP4.5) emission scenario.

The choice of downscaling method is also an important source of uncertainty in hydrological projections (Schmidli et al., 2007; Segui et al., 2010). The delta-change (DC) and DC-V statistical downscaling methods are widely used in streamflow projections (Immerzeel et al., 2010, 2012, 2013; Lutz et al., 2014; Su et al., 2016). Almost no differences were observed between the modeled mean climate data of the metrological stations over the baseline period (1971–2005) using the two downscaling methods. In addition, the modeled data matched the measured values well (not shown). The average annual hydrographs of streamflow simulated using downscaled historical GCM data adopting the DC-V and DC methods from 1971 to 1999 in the UB are shown in Fig. 14a. The simulation results using the two downscaled data are clearly close to the observations, thus supporting the reasonability of the downscaled historical and projected downscaled series. It is also difficult to judge which downscaling method can provide more realistic future climate projections because there is very little bias between the simulated historical streamflow sets. There are only small differences between the projected climate series from the two downscaled methods, with an average bias of 0.27 (0.39) °C for annual mean air temperature and 16.7 (20.5) mm for annual precipitation under the RCP2.6 (RCP4.5) scenario across our study catchments (Fig. 14b). The differences in two projected future climate sets resulted in a mean bias of 7.5 (9.8)%, 6.1 (6.1)% and 3.2 (3.7)% for projected mean streamflow, glacier runoff and glacier area under the two emission scenarios, respectively (Fig. 14c and d).

Overall, GCMs are the dominant source of uncertainty for projecting the streamflow, while *DDFs* are considered to be the largest source of uncertainty for glacier area and glacier meltwater projections. Therefore, glacier information must be used for model parameters calibration to effectively reduce the uncertainty in glacier projections. Although the uncertainties in glacier and stream projections are very apparent, the future runoff will likely increase due to increased precipitation, while glacier runoff is likely to reach its tipping point as a result of the rapid shrinkage of glaciers with climate warming.

5.4. Consequences of changes in the cryosphere and streamflow

Glaciers are expected to keep shrinking because of increasing air temperature. Although the contributions of glacier meltwater to streamflow are very limited in our study catchments, the role of glaciers in the regulation of streamflow should not be neglected, especially during the warm season, representing the peak period of water demand. As shown in Fig. 15, an obvious negative relationship occurred between glacier runoff and streamflow in the warm season for the five catchments, which indicates less glacier meltwater during wet years and more glacier meltwater during arid years. This phenomenon is commonly referred to as the glacier compensation effect (Zhao et al., 2015). In the extreme dry warm season, the glacier runoff contribution can reach 9–15% in the UYA, US and UB, where the contribution of glacier meltwater to the annual streamflow is less than 6% (Fig. 15b, d and e). With the retreating glaciers, the role of glaciers in streamflow regulation will diminish or even completely disappear, which will increase the risk of drought to hamper downstream agricultural activities.

Over the next century, the permafrost is expected to degrade as the thawing depth continues to increase because of the increasing air temperature during the warm season (Fig. 16a and c). A significant negative relationship was observed between the runoff coefficient and thawing depth of the permafrost area (Fig. 16b and d) in the UYE. Thus, the permafrost degradation and increase in thawing depth will allow for greater infiltration and water storage during the warm season, leading to a subsequent reduction of the runoff coefficient (Fig. 16a and c). Warming of the soil temperature will also lead to the formation of unfrozen zones within the permafrost, thus providing more baseflow in the cold season (Fig. 9). This phenomenon has also been reported by Niu et al. (2011) for rivers on the TP and Ye et al. (2009) for Arctic rivers.

Cold season discharge is expected to substantially increase due to the permafrost soil degradation and earlier snow/ice melt, whereas the warm season discharge may decrease if increases in precipitation are not sufficient to offset the decrease in the runoff coefficient and reduced snow/ice meltwater (Fig. 10c and f). In general, the water demand for agriculture is expected to increase due to higher temperatures. Such changes in streamflow may reduce the water supply for warm season downstream agriculture, which will have a considerable effect on food security. Thus, even more balanced water-resource management will be required.

6. Conclusions

In this work, we coupled glacier melting (enhanced degree-day) and glacier evolution (volume-area scaling law) schemes to the macroscale VIC hydrological model. The extended hydrological model (named VIC-CAS) can explicitly simulate glacier retreat or advance and all major cryospheric hydrological processes; therefore, it is suitable for hydrological simulation on the TP. To reduce uncertainties in simulations from model parameters, a progressive two-stage calibration strategy that jointly uses the remotely sensed glacier area and in-situ observed streamflow data was adopted to acquire more reliable model parameters. This model was applied to assess the climate change impacts on hydrology and project future change in the upstream regimes of the Yellow, Yangtze, Mekong, Salween, and Brahmaputra rivers on the TP.

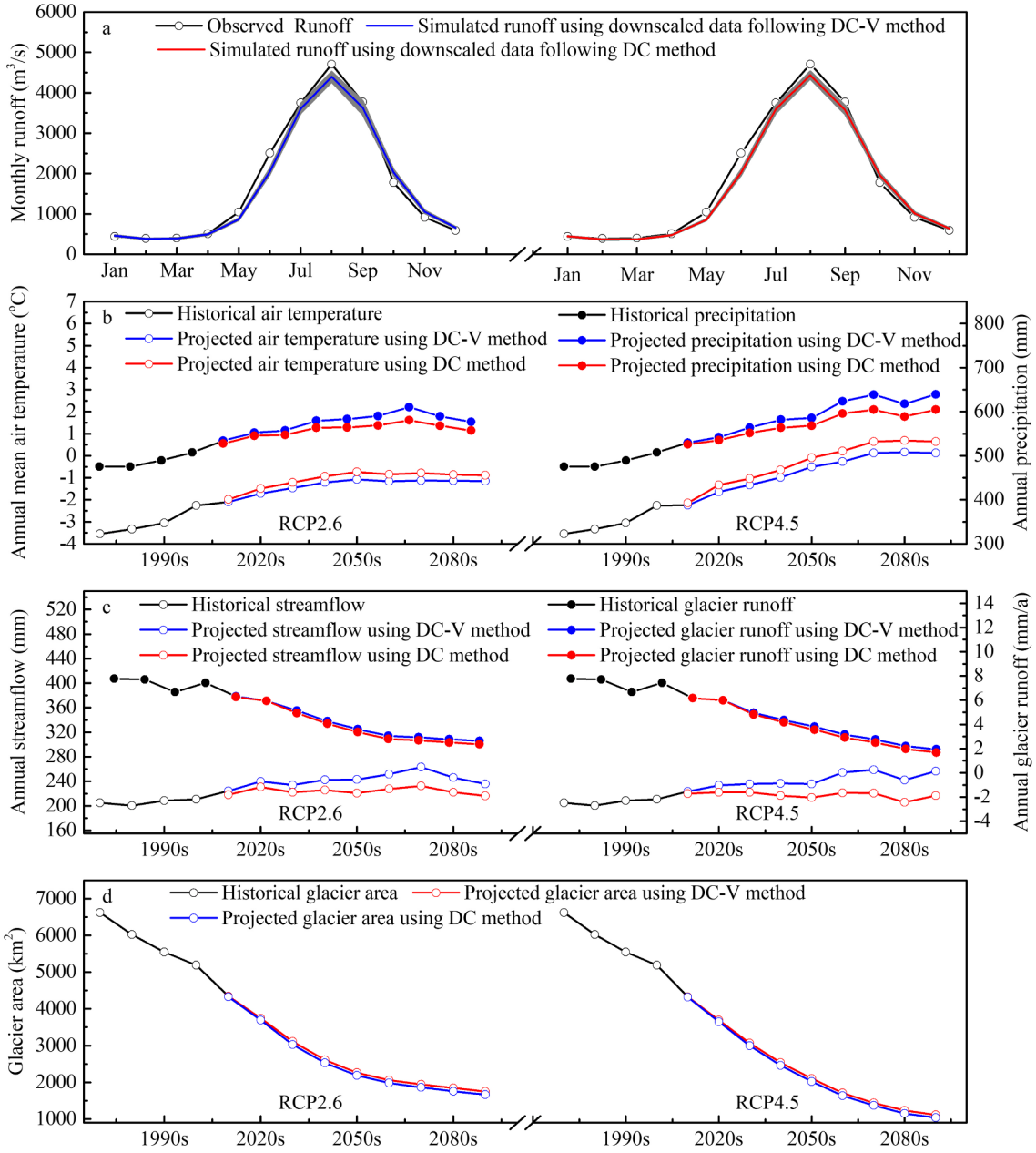

Fig. 14. Comparison of the simulated and projected results adopting the DC-V and DC downscaling methods. a Annual hydrographs of streamflow simulated using downscaled historical GCMs data, adopting two downscaling methods over 1971–1999 in the UB. The solid line represents the ensemble means, and the gray swath represents the spans of results from 5 GCMs. b, c and d Comparison of projections (air temperature, precipitation, streamflow, glacier runoff, and glacier area) adopting the two downscaling methods.

The following major conclusions are drawn.

(1) The extended VIC-CAS model allows an accurate simulation of both river flow and glacier evolution in the five large cryospheric catchments on the TP through the two-stage calibration strategy.
(2) The climate change analysis based on downscaled data from the five different GCMs suggests that the annual mean air temperature is projected to increase by 0.11 (0.31) °C per decade and precipitation by 6.6 (14.3) mm per decade under RCP2.6 (RCP4.5) global emission scenarios.
(3) With climate warming, glaciers are projected to retreat steadily. The results show that relative to 2010, the glacier area in 2100 will decline by 46.6 (62.1)%, 70.8 (80.9)%, 88.2 (95.6)%, 71.8 (79.6)%, and 60.0 (75.8)% for the UYE, UYA, UM, US, and UB, respectively. Glacier runoff is projected to start to decline in the UYA after the 2030 s, while glacier runoff was already beyond its tipping point at the beginning of the 21st century in UYE, UM, US, and UB, with the occurrence of greater than 20% glacier area loss from 1971 to 2010.
(4) Although large uncertainties are observed in the projections due to a high degree of uncertainty in future climate change from GCMs, annual streamflow is expected to increase due to an increase in rainfall runoff, which compensates for the expected decrease in glacier and snow melt water. The annual hydrograph remains unchanged, except for the UYE, where the peak streamflow will occur 1 month earlier because of earlier snowmelt and increased the rainfall/precipitation ratios. Due to the increase in thawing depth

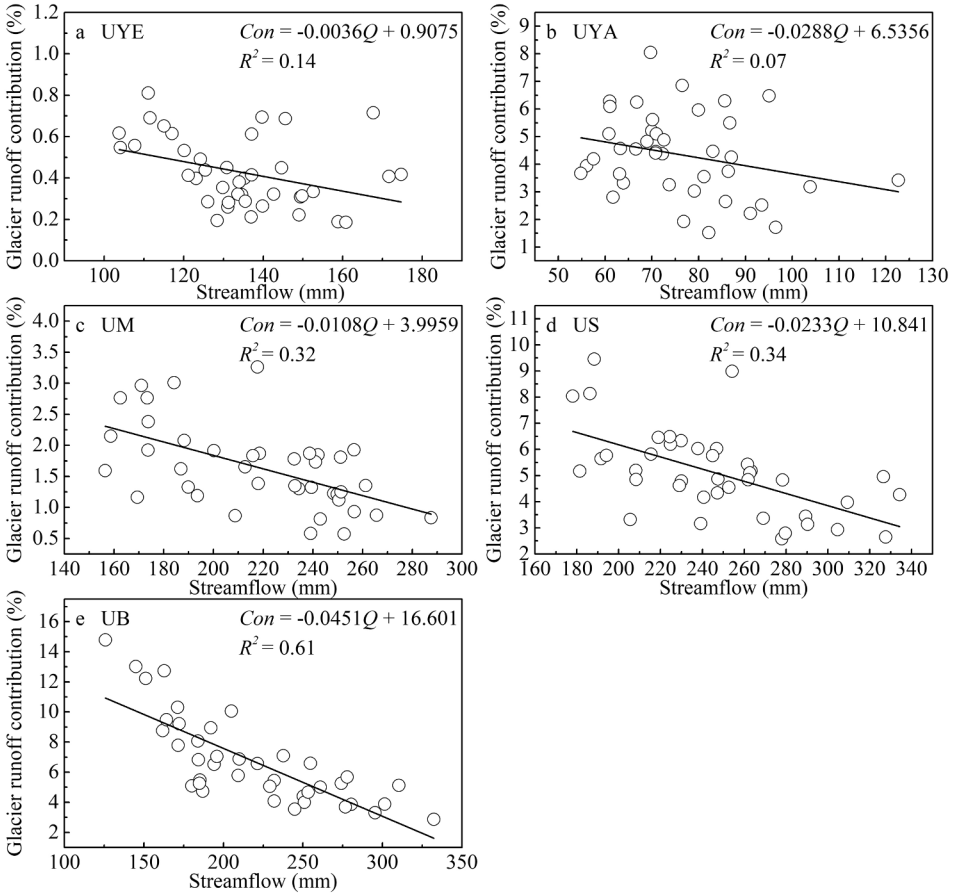

Fig. 15. Scatterplots of glacier melt water contribution (*Con*) versus streamflow (*Q*) during warm season (May–October) from the 1971 to 2010 for the UYE, UYA, UM, US, and UB basins. The solid line shows the linear relationship between the glacier runoff contribution and streamflow.

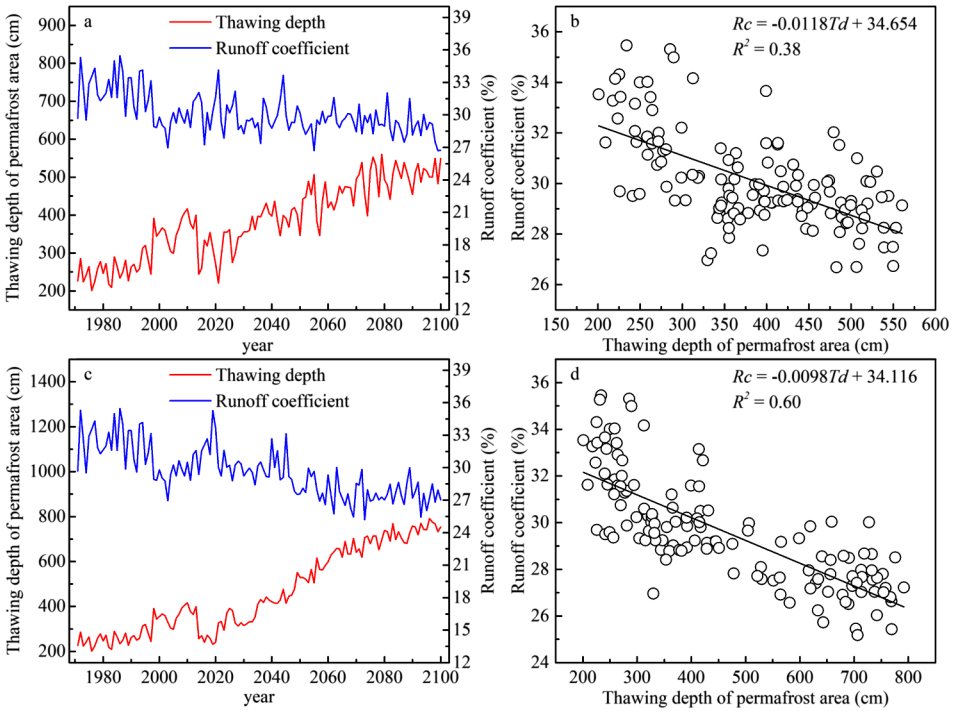

Fig. 16. Runoff coefficient and mean thawing depth of permafrost area changes (a and b) and scatterplots of the runoff coefficient versus thawing depth (c and d) during the warm season from 1971 to 2100 for the UYE. The projections in a and b were obtained under the RCP2.6 scenario, while the projections in c and d were obtained under the RCP4.5 scenario. The solid line shows the linear relationship between the runoff coefficient (*Rc*) and thawing depth (*Td*).

and earlier snow/ice melt, the cold season streamflow is projected to substantially increase. However, the warm season streamflow may decrease if the increases in precipitation are not sufficient to offset the reduced warm season runoff coefficient and snow/ice melt water.

Declaration of interests

The authors declare that they have no known competing financial interests.

Acknowledgements

This work was supported by the "Strategic Priority Research Program" of the Chinese Academy Sciences (XDA19070302) and National Nature Science Foundation of China (41871059, 41730751, 41671056, 41771087, 41471060and 41801036). The authors wish to thank the editors and the anonymous reviewers for all their helpful discussions and advice.

References

Bahr, D.B., Dyurgerov, M., Meier, M.F., 2009. Sea-level rise from glaciers and ice caps: a lower bound. Geophys. Res. Lett. 36, L03501. https://doi.org/10.1029/2008GL036309.

Bahr, D.B., 2011. Estimation of glacier volume and volume change by scaling methods. In: Singh, V.P., Singh, P., Haritashya, U.K. (Eds.), Encyclopedia of Snow, Ice and Glaciers. Encyclopedia of Earth Sciences Series. Springer, Dordrecht. https://doi.org/10.1007/978-90-481-2642-2.

Barria, P., Walsh, K.J.E., Peel, M.C., Karoly, D., 2015a. Uncertainties in runoff projections in southwestern Australian catchments using a global climate model with perturbed physics. J. Hydrol. 529, 184–199.

Barria, P., Walsh, K.J.E., Peel, M.C., Karoly, D., 2015b. Uncertainties in runoff projections in southwestern Australian catchments using a global climate model with perturbed physics. J. Hydrol. 529, 184–199. https://doi.org/10.1016/j.jhydrol.2015.07.040.

Berthier, E., Arnaud, Y., Kumar, R., Ahmad, S., Wagnon, P., Chevallier, P., 2007. Remote sensing estimates of glacier mass balances in the HimachalPradesh (Western Himalaya, India). Remote Sens. Environ. 108, 327–338.

Bouwer, L.M., Aerts, J.C.J.H., van de Coterlet, G.M., van de Giesen, N., Gieske, A., Mannaerts, C., 2004. Evaluating downscaling methods for preparing global circulation model (GCM) data for hydrological impact modelling. In: Aerts, J.C.J.H., Droogers, P. (Eds.), Climate Change in Contrasting River Basins. CABI Publishing, Wallingford, pp. 25–47.

Carenzo, M., Pellicciotti, F., Rimkus, S., Burlando, P., 2009. Assessing the transferability and robustness of an enhanced temperature-index glacier-melt model. J. Glaciol. 55 (190), 258–274.

Chen, X., Long, D., Hong, Y., Zeng, C., Yan, D.H., 2017a. Improved modeling of snow and glacier melting by a progressive two-stage calibration strategy with GRACE and multisource data: how snow and glacier meltwater contributes to the runoff of the Upper Brahmaputra River basin? Water Resour. Res. 53, 2431–2466.

Chen, Y., Li, W., Fang, G., Li, Z., 2017b. Review article: hydrological modeling in glacierized catchments of central Asia – status and challenges. Hydrol. Earth Syst. Sci. 21, 1–23.

Cherkauer, K.A., Lettenmaier, D.P., 2003. Simulation of spatial variability in snow and frozen soil. J. Geophys. Res. Atmos. 108 (D22), 1663–1675.

Chiew, F.H.S., et al., 2010. Comparison of runoff modelled using rainfall from different downscaling methods for historical and future climates. J. Hydrol. 387 (1–2), 10–23.

Cuo, L., Zhang, Y., 2017. Spatial patterns of wet season precipitation vertical gradients on the Tibetan Plateau and the surroundings. Sci. Rep. 7 (1), 5057. https://doi.org/10.1038/s41598-017-05345-6.

Cuo, L., Zhang, Y., Bohn, T.J., Zhao, L., Li, J., Liu, Q., Zhou, B., 2015. Frozen soil degradation and its effects on surface hydrology in the northern Tibetan Plateau. J. Geophys. Res. [Atmos.] 120, 8276–8298. https://doi.org/10.1002/2015JD023193.

Cuo, L., Zhang, Y., Wang, Q., Zhang, L., Zhou, B., Hao, Z., Su, F., 2013. Climate change on the Northern Tibetan Plateau during 1957–2009: spatial patterns and possible mechanisms. J. Clim. 26 (1), 85–109.

Cui, X.F., Graf, H.F., 2009. Recent land cover changes on the Tibetan Plateau: a review. Clim. Change 94 (1–2), 47–61.

Dan, L., Ji, J.J., Xie, Z.H., Chen, F., Wen, G., Richey, J.E., 2012. Hydrological projections of climate change scenarios over the 3H region of China: a VIC model assessment. J. Geophys. Res. 117, D11102. https://doi.org/10.1029/2011JD017131.

Duan, A.M., Xiao, Z.X., 2015. Does the climate warming hiatus exist over the Tibetan Plateau? Sci. Rep. 5, 13711. https://doi.org/10.1038/srep13711.

Ding, Y.H., Wang, Z.Y., Sun, Y., 2008. Inter-decadal variation of the summer precipitation in East China and its association with decreasing Asian summer monsoon. Part I: observed evidences. Int. J. Climatol. 28 (9), 1139–1161.

Duethmann, D., Bolch, T., Farinotti, D., Kriegel, D., Vorogushyn, S., Merz, B., Pieczonka, T., Jiang, T., Su, B., Güntner, A., 2015. Attribution of streamflow trends in snow and glacier melt-dominated catchments of the Tarim River, Central Asia. Water Resour. Res. 51 (6), 4727–4750.

Duethmann, D., Peters, J., Blume, T., Vorogushyn, S., Güntner, A., 2014. The value of satellite-derived snow cover images for calibrating a hydrological model in snow-dominated catchments in Central Asia. Water Resour. Res. 50 (3), 2002–2021.

Elsner, M.M., Cuo, L., Voisin, N., Deems, J.S., Hamlet, A.F., Vano, J.A., Mickelson, K.E.B., Lee, S.Y., Lettenmaier, D.P., 2010. Implications of 21st century climate change for the hydrology of Washington State. Clim. Change 102 (1–2), 225–260.

Elsner, M.M., Gangopadhyay, S., Pruitt, T., Brekke, L.D., Mizukami, N., Clark, M.P., 2014. How does the choice of distributed meteorological data affect hydrologic model calibration and streamflow simulations? J. Hydrometeorol. 15, 1384–1403. https://doi.org/10.1175/JHM-D-13-083.1.

Essery, R., Morin, S., Lejeune, Y., Ménard, C.B., 2013. A comparison of snow models using observations from an alpine site. Adv. Water Resour. 55, 131–148.

Feng, S., Hu, Q., Qian, W., 2004. Quality control of daily meteorological data in China (1951–2000): a new dataset. Int. J. Climatol. 24, 853–870.

Fujita, K., Ohta, T., Ageta, Y., 2007. Characteristics and climatic sensitivities of runoff from a cold-type glacier on the Tibetan Plateau. Hydrol. Process. 21 (21), 2882–2891.

Gao, H.K., Ding, Y.J., Zhao, Q.D., Hrachowitz, M., Savenije, H.H.G., 2017a. The importance of aspect for modelling the hydrological response in a glacier catchment in Central Asia. Hydrol. Process. 31 (16), 2842–2859.

Gao, H.K., Han, T.D., Liu, Y., Zhao, Q.D., 2017b. Use of auxiliary data of topography, snow and ice to improve model performance in a glacier-dominated catchment in Central Asia. Hydrol. Res. 48 (5), 1418–1437.

Gao, H.K., He, X.B., Ye, B.S., Pu, J.C., 2012. Modeling the runoff and glacier mass balance in a small watershed on the Central Tibetan Plateau, China, from 1955 to 2008. Hydrol. Process. 26 (11), 1593–1603.

Gao, H.L., Tang, Q.H., Shi, X.G., Zhu, C.M., Bohn, T.J., Su, F.G., Sheffield, J., Pan, M., Lettenmaier, D., Wood, E.F., 2009. Water-budget record from variable infiltration capacity (VIC) model. Dept. of Civil and Environmental Engineering, University of Washington, Seattle, WA.

Gao, T.G., Kang, S.C., Cuo, L., Zhang, T.J., Zhang, G.S., Zhang, Y.L., Sillanpaa, M., 2015. Simulation and analysis of glacier runoff and mass balance in the Nam Co basin, southern Tibetan Plateau. J. Glaciol. 61 (227), 447–460.

Gao, Y.H., Cuo, L., Zhang, Y.X., 2014. Changes in moisture flux over the Tibetan Plateau during 1979–2011 and possible Mechanisms. J. Clim. 27, 1876–1893.

Global Soil Data Task, 2014. Global Soil Data Products CD-ROM Contents (IGBP-DIS). Data Set. Available Online [http://daac.ornl.gov] from Oak Ridge National Laboratory Distributed Active Archive Center, Oak Ridge, Tennessee, U.S.A. https://doi.org/10.3334/ORNLDAAC/565.

Grinsted, A., 2013. An estimate of global glacier volume. Cryosphere 7 (1), 141–151.

Guo, D.L., Wang, H.J., 2012. The significant climate warming in the northern Tibetan Plateau and its possible causes. Int. J. Climatol. 32 (12), 1775–1781.

Guo, X.Y., Wang, L., Tian, L.D., 2016. Spatio-temporal variability of vertical gradients of major meteorological observations around the Tibetan Plateau. Int. J. Climatol. 36 (4), 1901–1916.

Guo, W.Q., Liu, S.Y., Xu, J.L., Wu, L.Z., Shangguan, D.H., Yao, X.J., Wei, J.F., Bao, W.J., Yu, P.C., Liu, Q., Jiang, Z.L., 2015. The second Chinese glacier inventory: data, methods and results. J. Glaciol. 61 (226), 357–372.

Hansen, M.C., Defries, R.S., Townshend, J.R.G., Sohlberg, R., 2000. Global land cover classification at 1 km spatial resolution using a classification tree approach. Int. J. Remote Sens. 21 (6–7), 1331–1364.

Hidalgo, H.G., Amador, J.A., Alfaro, E.J., Quesada, B., 2013. Hydrological climate change projections for Central America. J. Hydrol. 495, 94–112.

Hock, R., 2003. Temperature index melt modelling in mountain areas. J. Hydrol. 282 (1–4), 104–115.

Hock, R., 2005. Glacier melt: a review of processes and their modelling. Prog. Phys. Geogr. 29 (3), 362–391.

Hock, R., Holmgren, B., 2005. A distributed surface energy-balance model for complex topography and its application to Storglaciaren, Sweden. J. Glaciol. 51 (172), 25–36.

Hu, Q., Jiang, D.B., Fan, G.Z., 2014. Evaluation of CMIP5 models over the Qinghai-Tibetan Plateau. Chin. J. Atmos. Sci. 38 (5), 15.

Huang, J., Kang, S.C., Zhang, Q.G., Jenkins, M.G., Guo, J.M., Zhang, G.S., Wang, K., 2012. Spatial distribution and magnification processes of mercury in snow from high-elevation glaciers in the Tibetan Plateau. Atmos. Environ. 46, 140–146.

Huss, M., Farinotti, D., 2012. Distributed ice thickness and volume of all glaciers around the globe. J. Geophys. Res. 117, F04010. https://doi.org/10.1029/2012JF002523.

Huss, M., Farinotti, D., Bauder, A., Funk, M., 2008. Modelling runoff from highly glacierized alpine drainage basins in a changing climate. Hydrol. Process. 22 (19), 3888–3902.

Huss, M., Zemp, M., Joerg, P.C., Salzmann, N., 2014. High uncertainty in 21st century runoff projections from glacierized basins. J. Hydrol. 510, 35–48.

Hwang, S., Graham, W.D., 2013. Development and comparative evaluation of a stochastic analog method to downscale daily GCM precipitation. Hydrol. Earth Syst. Sci. 17, 4481–4502.

Immerzeel, W.W., Pellicciotti, F., Bierkens, M.F.P., 2013. Rising river flows throughout the twenty-first century in two Himalayan glacierized watersheds. Nat. Geosci. 6 (9), 742–745.

Immerzeel, W.W., van Beek, L.P.H., Bierkens, M.F.P., 2010. Climate change will affect the asian water towers. Science 328 (5984), 1382–1385.

Immerzeel, W.W., van Beek, L.P.H., Konz, M., Shrestha, A.B., Bierkens, M.F.P., 2012. Hydrological response to climate change in a glacierized catchment in the Himalayas. Clim. Change 110 (3–4), 721–736.

Jeelani, G., Feddema, J.J., van der Veen, C.J., Stearns, L., 2012. Role of snow and glacier melt in controlling river hydrology Liddar watershed in the (western Himalaya) under current and future climate. Water Resour. Res. 48 (W12508), 1–16.

Kang, S.C., Xu, Y.W., You, Q.L., Flügel, W., Pepin, N., Yao, T.D., 2010. Review of climate

and cryospheric change in the Tibetan Plateau. Environ. Res. Lett. 5, 015101. https://doi.org/10.1088/1748-9326/5/1/015101.
Konz, M., Seibert, J., 2010. On the value of glacier mass balances for hydrological model calibration. J. Hydrol. 385 (1), 238–246.
Konz, M., Uhlenbrook, S., Braun, L., Shrestha, A., Demuth, S., 2007. Implementation of a process-based catchment model in a poorly gauged, highly glacierized Himalayan headwater. Hydrol. Earth Syst. Sci. 11 (4), 1323–1339.
Kotlarski, S., Jacob, D., Podzun, R., Paul, F., 2010. Representing glaciers in a regional climate model. Clim. Dyn. 34 (1), 27–46.
Lawrence, D.M., Slater, A.G., 2005. A projection of severe near-surface permafrost degradation during the 21st century. Geophys. Res. Lett. 32 (24), 1–5. https://doi.org/10.1029/2005GL025080.
Lemke, P., Ren, J., Alley, R.B., Allison, I., Carrasco, J., Flato, G., Fujii, Y., Kaser, G., Mote, P., Thomas, R.H., Zhang, T., 2007. Observations: changes in snow, ice and frozen ground. In: Solomon, S., Qin, D., Manning, M., Chen, Z., Marquis, M., Averyt, K.B., Tignor, M., Miller, H.L. (Eds.), Climate Change 2007: The Physical Science Basis. Contribution of Working Group I to the Fourth Assessment Report of the Intergovernmental Panel on Climate. Change. Cambridge University Press, Cambridge, UK, pp. 338–383.
Li, F.P., Zhang, Y.Q., Xu, Z.X., Teng, J., Liu, C.M., Liu, W.F., Mpelasoka, F., 2013. The impact of climate change on runoff in the southeastern Tibetan Plateau. J. Hydrol. 505, 188–201.
Li, F.P., Zhang, Y.Q., Xu, Z.X., Liu, C.M., Zhou, Y.C., Liu, W.F., 2014. Runoff predictions in ungauged catchments in southeast Tibetan Plateau. J. Hydrol. 511, 28–38.
Li, X., Cheng, G.D., Jin, H.J., Kang, E.S., Che, T., Jin, R., Wu, L.Z., Nan, Z.T., Wang, J., Shen, Y.P., 2008. Cryospheric change in China. Global Planet. Change 62, 210–218.
Li, Z.X., He, Y.Q., Pu, T., Jia, W.X., He, X.Z., Pang, H.X., Zhang, N.N., Liu, Q., Wang, S.J., Zhu, G.F., Wang, S.X., Chang, L., Du, J.K., Xin, H.J., 2010. Changes of climate, glaciers and runoff in China's monsoonal temperate glacier region during the last several decades. Quat. Int. 218 (1–2), 13–28.
Liang, X., Wood, E.F., Lettenmaier, D.P., 1996. Surface soil moisture parameterization of the VIC-2L model: evaluation and modification. Global Planet. Change 13 (1–4), 195–206.
Liu, L.L., Liu, Z.F., Ren, X.Y., Fischer, T., Xu, Y., 2011. Hydrological impacts of climate change in the Yellow River Basin for the 21st century using hydrological model and statistical downscaling model. Quat. Int. 244 (2), 211–220.
Liu, S.Y., Sun, W.X., Shen, Y.P., Li, G., 2003. Glacier changes since the Little Ice Age maximum in the western Qilian Shan, northwest China, and consequences of glacier runoff for water supply. J. Glaciol. 49 (164), 117–124.
Liu, S.Y., Yao, X.J., Guo, W.Q., Xu, J.L., Shangguan, D.H., Wei, J.F., Bao, W.J., Wu, L.Z., 2015a. The contemporary glaciers in China based on the second Chinese glacier inventory. Acta Geogr. Sinica 70 (1), 3–16.
Liu, W.F., Xu, Z.X., Li, F.P., Zhang, L.Y., Zhao, J., Yang, H., 2015b. Impacts of climate change on hydrological processes in the Tibetan Plateau: a case study in the Lhasa River basin. Stoch. Environ. Res. Risk A 29 (7), 1809–1822.
Lohmann, D., Nolte-Holube, R., Raschke, E., 1996. A large-scale horizontal routing model to be coupled to land surface parameterization schemes. Tellus 48, 708–721.
Lohmann, D., Raschke, E., Nijssen, B., Lettenmaier, D.P., 1998. Regional scale hydrology: I. Formulation of the VIC-2L model coupled to a routing model. Hydrol. Sci. J. 43, 131–141.
Lu, W.J., Wang, W.G., Shao, Q.X., Yu, Z.B., Hao, Z.C., Xing, W.Q., Yong, B., Li, J.X., 2018. Hydrological projections of future climate change over the source region of Yellow River and Yangtze River in the Tibetan Plateau: a comprehensive assessment by coupling RegCM4 and VIC model. Hydrol. Process. 32 (13), 2096–2117.
Luo, Y., Arnold, J., Liu, S., Wang, X., Chen, X., 2013. Inclusion of glacier processes for distributed hydrological modeling at basin scale with application to a watershed in Tianshan Mountains, northwest China. J. Hydrol. 477 (16), 72–85.
Lutz, A.F., Immerzeel, W.W., Shrestha, A.B., Bierkens, M.F.P., 2014. Consistent increase in High Asia's runoff due to increasing glacier melt and precipitation. Nat. Clim. Change 4 (7), 587–592.
MacDougall, A.H., Wheler, B.A., Flowers, G.E., 2011. A preliminary assessment of glacier melt-model parameter sensitivity and transferability in a dry subarctic environment. Cryosphere 5 (4), 1011–1028.
Miao, C.Y., Duan, Q.Y., Yang, L., Borthwick, A.G.L., 2012. On the applicability of temperature and precipitation data from CMIP3 for China. PLoS One 7 (9), e44659. https://doi.org/10.1371/journal.pone. 0044659.
Möller, M., Schneider, C., 2010. Calibration of glacier volume-area relations from surface extent fluctuations and application to future glacier change. J. Glaciol. 56, 33–40.
Moradkhani, H., Hsu, K.L., Gupta, H., Sorooshian, S., 2005. Uncertainty assessment of hydrologic model states and parameters: sequential data assimilation using the particle filter. Water Resour. Res. 41 (5), 237–246.
Nan, Z.T., Li, S.X., Cheng, G.D., 2005. Prediction of permafrost distribution on the Qinghai-Tibet Plateau in the next 50 and 100 years. Sci. China Ser. D 48 (6), 797–804.
Nijssen, B., Schnur, R., Lettenmaier, D.P., 2001. Global retrospective estimation of soil moisture using the variable infiltration capacity land surface model, 1980–93. J. Clim. 14 (8), 1790–1808.
Niu, L., Ye, B.S., Li, J., Sheng, Y., 2011. Effect of permafrost degradation on hydrological processes in typical basins with various permafrost coverage in Western China. Sci. China Earth Sci. 54 (4), 615–624.
Peel, M.C., Srikanthan, R., McMahon, T.A., Karoly, D.J., 2015. Approximating uncertainty of annual runoff and reservoir yield using stochastic replicates of global climate model data. Hydrol. Earth Syst. Sci. 19 (4), 1615–1639.
Pellicciotti, F., Ragettli, S., Carenzo, M., McPhee, J., 2013. Changes of glaciers in the Andes of Chile and priorities for future work. Sci. Total Environ. 493, 1197–1210.
Price, D.T., McKenney, D.W., Nalder, I.A., Hutchinson, M.F., Kesteven, J.L., 2000. A comparison of two statistical methods for spatial interpolation of Canadian monthly mean climate data. Agric. Forest Meteorol. 101 (2–3), 81–94.
Radić, V., Hock, R., Oerlemans, J., 2007. Volume-area scaling vs flowline modelling in glacier volume projections. Ann. Glaciol. 46 (1), 234–240.
Radić, V., Hock, R., 2010. Regional and global volumes of glaciers derived from statistical upscaling of glacier inventory data. J. Geophys. Res. 115, F01010. https://doi.org/10.1029/2009JF001373.
Radić, V., Hock, R., 2014. Glaciers in the earth's hydrological cycle: assessments of glacier mass and runoff changes on global and regional scales. Surv. Geophys. 35, 813–837.
Ramanathan, V., Carmichael, G., 2008. Global and regional climate changes due to black carbon. Nat. Geosci. 1 (4), 221–227.
Raper, S.C.B., Braithwaite, R.J., 2005. The potential for sea level rise: new estimates from glacier and ice cap area and volume distributions. Geophys. Res. Lett. 32, L05502. https://doi.org/10.1029/2004GL021981.
Raper, S.C.B., Braithwaite, R.J., 2006. Low sea level rise projections from mountain glaciers and icecaps under global warming. Nature 439 (7074), 311–313.
Rees, H.G., Collins, D.N., 2006. Regional differences in response of flow in glacier-fed Himalayan rivers to climatic warming. Hydrol. Process. 20 (10), 2157–2169.
Schaefli, B., Huss, M., 2011. Integrating point glacier mass balance observations into hydrologic model identification. Hydrol. Earth Syst. Sci. 15 (4), 1227–1241.
Schmidli, J., Goodess, C.M., Frei, C., Haylock, M.R., Hundecha, Y., Ribalaygua, J., Schmith, T., 2007. Statistical and dynamical downscaling of precipitation: An evaluation and comparison of scenarios for the European Alps. J. Geophys. Res. 112. https://doi.org/10.1029/2005JD007026.
Segui, P.Q., Ribes, A., Martin, E., Habets, F., Boe, J., 2010. Comparison of three downscaling methods in simulating the impact of climate change on the hydrology of Mediterranean basins. J. Hydrol. 383 (1–2), 111–124.
Shi, P.H., Duan, K.Q., Liu, H.C., Yang, J.H., Zhang, X., Sun, J.Y., 2016. Response of Xiao Dongkemadi Glacier in the central Tibetan Plateau to the current climate change and future scenarios by 2050. J. Mt. Sci. 13 (1), 13–28.
Shi, Y.F., Liu, C.H., Kang, E.S., 2009. The glacier inventory of China. Ann. Glaciol. 50 (53), 1–4.
Shrestha, M., Wang, L., Koike, T., Tsutsui, H., Xue, Y., Hirabayashi, Y., 2014. Correcting basin-scale snowfall in a mountainous basin using a distributed snowmelt model and remote-sensing data. Hydrol. Earth Syst. Sci. 18, 747–761.
Song, M.H., Zhou, C.P., Ouyang, H., 2004. Distributions of dominant tree species on the Tibetan Plateau under current and future climate scenarios. Mt. Res. Dev. 24 (2), 166–173.
Stahl, K., Moore, R.D., Shea, J.M., Hutchinson, D., Cannon, A.J., 2008. Coupled modelling of glacier and streamflow response to future climate scenarios. Water Resour. Res. 44, W02422. https://doi.org/10.1029/2007WR005956.
Su, F., Zhang, L., Qu, T., Chen, D., Yao, T., Tong, K., Qi, Y., 2016. Hydrological response to future climate changes for the major upstream river basins in the Tibetan Plateau. Global Planet. Change 136, 82–95.
Su, F.G., Duan, X.L., Chen, D.L., Hao, Z.H., Cuo, L., 2013. Evaluation of the global climate models in the CMIP5 over the Tibetan Plateau. J. Clim. 26 (10), 3187–3208.
Tahir, A.A., Chevallier, P., Arnaud, Y., Neppel, L., Ahmad, B., 2011. Modeling snowmelt-runoff under climate scenarios in the Hunza River basin, Karakoram Range, Northern Pakistan. J. Hydrol. 409 (1–2), 104–117.
Teng, J., Vaze, J., Chiew, F.H.S., Wang, B., Perraud, J.M., 2012. Estimating the relative uncertainties sourced from GCMs and hydrological models in modeling climate change impact on runoff. J. Hydrometeorol. 13 (1), 122–139.
Tong, K., Su, F.G., Yang, D.Q., Zhang, L.L., Hao, Z.C., 2014. Tibetan Plateau precipitation as depicted by gauge observations, reanalyses and satellite retrievals. Int. J. Climatol. 34 (2), 265–285.
Van de Wal, R., Wild, M., 2001. Modelling the response of glaciers to climate change by applying volumearea scaling in combination with a high resolution GCM. Clim. Dynam. 18 (3–4), 359–366.
Wang, B., Bao, Q., Hoskins, B., Wu, G.X., Liu, Y.M., 2008. Tibetan Plateau warming and precipitation changes in east Asia. Geophys. Res. Lett. 35, L14702.
Wang, W.G., Li, J.X., Yu, Z.B., Ding, Y.M., Xing, W.Q., Lu, W.J., 2018. Satellite retrieval of actual evapotranspiration in the Tibetan Plateau: components partitioning, multi-decadal trends and dominated factors identifying. J. Hydrol. 559, 471–485.
Wei, J.F., Liu, S.Y., Guo, W.Q., Yao, X.J., Xu, J.L., Bao, W.J., Jiang, Z.L., 2014. Surface-area changes of glaciers in the Tibetan Plateau interior area since the 1970s using recent Landsat images and historical maps. Ann. Glaciol. 55 (66), 213–222.
Yang, K., Wu, H., Qin, J., Lin, C.G., Tang, W.J., Chen, Y.Y., 2014. Recent climate changes over the Tibetan Plateau and their impacts on energy and water cycle: a review. Global Planet. Change 112, 79–91.
Yao, T.D., Wang, Y.Q., Liu, S.Y., Pu, J.C., Shen, Y.P., Lu, A.X., 2004. Recent glacial retreat in High Asia in China and its impact on water resource in Northwest China. Sci. China Ser. D 47 (12), 1065–1075.
Ye, B.J., Feng, H.Y., Zhao, J.H., Fang, J., Shen, W.G., 2013. Microcalorimetry study on the microbial activity of permafrost on the Tibetan plateau of China. J. Therm. Anal. Calorim. 111 (3), 1731–1736.
Ye, B.S., Yang, D.Q., Zhang, Z.L., Kane, D.L., 2009. Variation of hydrological regime with permafrost coverage over Lena Basin in Siberia. J. Geophys. Res. 114 (D7), 1291–1298.
Ye, Q.H., Yao, T.D., Naruse, R., 2008. Glacier and lake variations in the Mapam Yumco basin, western Himalaya of the Tibetan Plateau, from 1974 to 2003 using remote-sensing and GIS technologies. J. Glaciol. 54 (188), 933–935.
Ye, Q.H., Zhu, L.P., Zheng, H.X., Naruse, R., Zhang, X.Q., Kang, S.C., 2007. Glacier and lake variations in the Yamzhog Yumco basin, southern Tibetan Plateau, from 1980 to 2000 using remote-sensing and GIS technologies. J. Glaciol. 53 (183), 673–676.
Zhang, L.L., Su, F.G., Yang, D.Q., Hao, Z.C., Tong, K., 2013. Discharge regime and simulation for the upstream of major rivers over Tibetan Plateau. J. Geophys. Res.

Atmos. 118 (15), 8500–8518.
Zhang, R.H., Su, F.G., Jiang, Z.H., Gao, X.J., Guo, D.L., Ni, J., You, Q.L., Lan, C., Zhou, B.T., 2015. An overview of projected climate and environmental changes across the Tibetan Plateau in the 21st century (in Chinese). Chin. Sci. Bull. 60 (32), 3036–3047.
Zhang, S.Q., Ye, B.S., Liu, S.Y., Zhang, X.W., Hagemann, S., 2012. A modified monthly degree-day model for evaluating glacier runoff changes in China. Part I: model development. Hydrol. Process 26 (11), 1686–1696.
Zhang, T.J., 2007. Perspectives on environmental study of response to climatic and land Cover/Land use change over the Qinghai-Tibetan plateau: an introduction. Arct. Antarct. Alp. Res. 39 (4), 631–634.
Zhang, Y., Liu, S.Y., Xu, J.L., Shangguan, D.H., 2008. Glacier change and glacier runoff variation in the Tuotuo River basin, the source region of Yangtze River in western China. Environ. Geol. 56 (1), 59–68.
Zhao, Q.D., Ye, B.S., Ding, Y.J., Zhang, S.Q., Yi, S.H., Wang, J., Shangguan, D.H., Zhao, C.C., Han, H.D., 2013. Coupling a glacier melt model to the Variable Infiltration Capacity (VIC) model for hydrological modeling in north-western China. Environ. Earth Sci. 68 (1), 87–101.
Zhao, Q.D., Zhang, S.Q., Ding, Y.J., Wang, J., Han, H.D., Xu, J.L., Zhao, C.C., Guo, W.Q., Shangguan, D.H., 2015. Modeling hydrologic response to climate change and shrinking glaciers in the highly glacierized Kunma Like River Catchment, Central Tian Shan. J. Hydrometeorol. 16 (6), 2383–2402.
Zhong, L., Su, Z.B., Ma, Y.M., Salama, M.S., Sobrino, J.A., 2011. Accelerated changes of environmental conditions on the Tibetan Plateau caused by climate change. J. Clim. 24 (24), 6540–6550.